Regenerative growth is constrained by *brain tumor* to ensure proper patterning in *Drosophila*

Syeda Nayab Fatima Abidi[1] and Rachel K. Smith-Bolton[1,*]

[1] Department of Cell and Developmental Biology, University of Illinois Urbana-Champaign, Urbana, IL 61801, USA

* rsbolton@illinois.edu

Abstract

Some animals respond to injury by inducing new growth to regenerate the lost structures. This regenerative growth must be carefully controlled and constrained to prevent overgrowth and to allow correct organization of the regenerating tissue. However, the factors that restrict regenerative growth have not been identified. Using a genetic ablation system in the *Drosophila* wing imaginal disc, we have identified one mechanism that constrains regenerative growth, impairment of which leads to erroneous patterning of the final appendage. Regenerating discs with reduced levels of the RNA-regulator Brain tumor (Brat) exhibit enhanced regeneration, but produce adult wings with disrupted margins that are missing extensive tracts of sensory bristles. In these mutants, aberrantly high expression of the pro-growth factor Myc and its downstream targets leads to loss of cell-fate specification. Thus, Brat ensures that the regenerating tissue forms the proper final structure by constraining expression of pro-regeneration genes.

Introduction

Regeneration is the remarkable process by which some organisms replace tissues and organs after damage such that both morphology and function are restored. Complete regeneration requires several steps to occur correctly including wound healing, cell proliferation, and proper patterning and cell-fate specification in the newly formed tissue. The degree of regenerative capacity varies among different species, ranging from whole-body regeneration in hydra and planaria to limited tissue regeneration in

mammals. Work in several model organisms has identified signaling pathways and molecular mechanisms that are important for initiating and executing regenerative growth after tissue damage, including JNK signaling (Bergantiños et al., 2010; Bosch et al., 2010, 2005; Martín et al., 2017; Tasaki et al., 2011), JAK/STAT signaling (Bando et al., 2013; Katsuyama et al., 2015; Verghese and Su, 2017), EGFR signaling (Fan et al., 2014; Jiang et al., 2011; Jin et al., 2015; Nakamura et al., 2007), Hippo signaling (Bando et al., 2009; Grijalva et al., 2014; Grusche et al., 2011; Hayashi et al., 2014; Sun and Irvine, 2011), Wnt signaling (Hanovice et al., 2019; Hobmayer et al., 2000; Kawakami et al., 2006; McClure and Schubiger, 2008; Schubiger et al., 2010; Smith-Bolton et al., 2009; Wehner et al., 2014), and Myc (Harris et al., 2016; Smith-Bolton et al., 2009). Many of these mechanisms are also important during normal development, and the process of regeneration was traditionally thought to be a redeployment of earlier developmental steps (Bosch et al., 2010; Gupta et al., 2013; Harris et al., 2016; Mader and Cameron, 2004; Muneoka and Bryant, 1982; Nakamura et al., 2007; Roensch et al., 2013). However, recent evidence suggests that regeneration is not a simple reiteration of development but can employ regeneration-specific regulatory mechanisms (Bosch et al., 2010; Harris et al., 2016; Luttrell et al., 2016; McCusker and Gardiner, 2013; Myohara, 2004; Schuster and Smith-Bolton, 2015; Vizcaya-Molina et al., 2018). Indeed, faithful regeneration likely requires additional mechanisms, since regrowth happens in the presence of wound-response signaling and in a developed juvenile or adult organism. Additionally, pro-growth pathways that are used during normal development are often activated in new ways and at higher strengths in the regenerating tissue (Bergantiños et al., 2010; Grusche et al., 2011; Katsuyama et al.,

2015; Smith-Bolton et al., 2009). These augmented pro-growth signals must be constrained as regeneration progresses to prevent overgrowth and to enable re-establishment of pattern and cell-fate specification. Thus, growth suppressors and additional patterning factors are likely used to terminate regeneration and allow differentiation (Sun and Irvine, 2014). However, despite our understanding of the pro-growth signals needed for regeneration, we do not yet know what factors exist in different model organisms to restrain growth and promote re-patterning of regenerating tissue.

Drosophila melanogaster imaginal discs, precursors of adult fly appendages, are simple columnar epithelia that have well-characterized, complex expression of patterning genes that determine cell-fate specification. Imaginal discs undergo regeneration after damage (Hariharan and Serras, 2017), and we have previously used a genetic ablation system to study patterning in the regenerating tissue (Schuster and Smith-Bolton, 2015; Smith-Bolton et al., 2009). Here we identify the RNA-regulator Brain tumor (Brat) as a key constraint on regenerative growth that ensures proper formation of the regenerated structure. Brat is a member of the TRIM- (tripartite motif containing)-NHL (NCL-1, HT2A, and LIN-41) family of proteins and functions as a translational repressor by binding to its target RNAs either independently or in a complex with Pumilio and Nanos (Loedige et al., 2015, 2014; Sonoda and Wharton, 2001). It acts as a potent differentiation factor and tumor suppressor in neural and ovarian germline stem cell lineages (Arama et al., 2000; Betschinger et al., 2006; Harris et al., 2011; Lee et al., 2006). Human and mouse orthologs of Brat, TRIM3 and TRIM32 respectively, also possess tumor-suppressor

activity in glioblastomas and are required for neuronal and muscle differentiation (Chen et al., 2014; Kudryashova et al., 2012; Nicklas et al., 2012; Schwamborn et al., 2009).

We show that regenerating wing imaginal discs with reduced levels of Brat regenerate better than controls, but the resulting adult wings have a disrupted margin. The margin loses some of the characteristic sensory bristles and veins, demonstrating an error in cell-fate specification. Importantly, these phenotypes are regeneration-specific, as they are not observed in the mutant animals after normal development. The enhanced regeneration is due to increased expression of the growth regulators Myc and Wingless as well as upregulation of *ilp8,* which delays metamorphosis and allows the damaged tissue more time to regenerate. Intriguingly, this seemingly beneficial elevated Myc expression is also responsible for the aberrant cell-fate specification at the wing margin, through misregulation of downstream target genes, including Chronologically inappropriate morphogenesis (Chinmo). Hence, Brat acts as an important growth regulator and protective factor by constraining Myc and Chinmo levels during regeneration to prevent errors in patterning, cell-fate specification, and differentiation in the regenerating tissue.

Results

Brat suppresses regenerative growth and is required for wing margin cell-fate specification during regeneration

To identify genes important for regenerative growth and re-patterning, we performed a candidate screen, using our wing imaginal disc ablation system (Smith-Bolton et al., 2009). The primordial wing was targeted for ablation at the early third-instar larval stage by using *rotund-GAL4* to drive the expression of the proapoptotic gene *reaper* for 24 hours (Figure 1A). Our ability to restrict damage to 24 hours was provided by *tubulin-GAL80^{ts}*, which can inhibit GAL4 activity at 18°C, but allows GAL4-driven cell death at 30°C in the 24-hour window. The extent of wing imaginal disc regeneration in the larvae was reflected in the adult wing size. Hence, the resulting adult wings were scored based on size and patterning features to identify mutants that affect genes that are involved in regulating regenerative growth and establishment of cell fates. There is inherent variability in this system because of its sensitivity to environmental conditions such as temperature, humidity, and food quality, causing the results of different experiments to vary slightly (Brock et al., 2017; Khan et al., 2017; Skinner et al., 2015; Sun and Irvine, 2011; Vonesch et al., 2016). Animals with the same genotype within an experiment also showed some variation, due to stochastic differences in the time each animal takes to eclose, with animals that take longer to eclose having larger wings (Khan et al., 2017; Smith-Bolton et al., 2009). However, differences between control and mutant animals using this system are reproducible, consistent, and have identified key regeneration genes (Brock et al., 2017; Khan et al., 2017; Schuster and Smith-Bolton, 2015; Skinner et al., 2015).

Using this genetic ablation system, we identified the gene *brain tumor (brat)* as an important regulator of regenerative growth. *brat^{1}*/+ mutants that did not experience

damage during development had adult wings that were not significantly different in size from controls (Figure S1A). However, after ablation and regeneration were induced, *brat*^{1}/+ mutants showed enhanced regeneration and had adult wings that were, on average, much larger than controls that had also undergone regeneration (Figure 1B and 1C). We confirmed this enhanced regeneration phenotype in heterozygotes for three other *brat* mutant alleles: *brat*^{192}, *brat*^{150} (Luschnig et al., 2004) and *brat*^{11} (Wright et al., 1981)(Figure S1B).

Interestingly, we also discovered a role for *brat* in cell-fate specification during regeneration. After normal development, *brat*^{1}/+ mutants had adult wings that were patterned normally (Figure 1D-E and Figure S1C). To confirm that loss of *brat* does not cause patterning errors during normal development, we knocked down Brat levels in the entire wing pouch using *brat* RNAi, which resulted in adult wings that were patterned normally (Figure S1D and S1E). A previous study in which Brat levels were reduced in the anterior and posterior compartments of the wing also did not report any patterning defects (Ferreira et al., 2014). However, when discs were ablated and allowed to regenerate, *brat* heterozygous mutant wings showed aberrant patterning such that the wing margin lost sensory bristles and vein material (Figure 1F and 1G). By contrast, control regenerated wings lost margin tissue at a lower frequency (Figure 1H and 1I). Furthermore, the extent of margin tissue lost was not as severe in control regenerated wings as compared to *brat*^{1}/+ regenerated wings (Figure 1H and 1I). Similar to the enhanced regeneration seen in *brat* mutants, we confirmed the loss-of-margin defect in heterozygotes for the additional three mutant alleles (Figure S1F).

136

137 ***brat* regulates entry into metamorphosis**

138 Tissue damage in imaginal discs can induce a systemic response in the larvae, which
139 extends the larval phase of development and delays pupariation (Halme et al., 2010;
140 Smith-Bolton et al., 2009). This delay in pupariation is due to expression of the relaxin-
141 like peptide *ilp8* in damaged discs (Colombani et al., 2012; Garelli et al., 2012). To
142 determine whether *brat* mutants regenerated better due to an enhanced delay in
143 pupariation, we measured rates of pupariation in control and mutant animals. We found
144 that during normal development, control and $brat^{1}$/+ animals pupariated at the same
145 time, indicating that the two genotypes develop at similar rates (Figure S2A). After disc
146 damage, *brat* mutants delayed pupariation an additional day compared to controls in
147 which discs were also damaged (Figure 2A and Figure S2B). Note that direct
148 comparisons cannot be made between regenerating larvae that spent 24 hours at 30°C
149 (Figure 2A, Figure S2B) and normally developing larvae that remain at 18°C (Figure
150 S2A), due to the effects of temperature on development. Our data show that *brat*/+
151 mutants are able to stay in the larval stage even longer than controls, giving them more
152 time to regenerate.

153

154 To determine why discs with reduced Brat had an increased delay in pupariation, we
155 measured *ilp8* transcript levels through qPCR. Undamaged control animals express
156 very low *ilp8* levels. However, after regeneration was induced, we saw an 80-fold
157 increase in *ilp8* levels in controls, while the $brat^{1}$/+ animals showed a 140-fold increase

158 (Figure 2B). Thus, *brat* suppresses *ilp8* during regeneration, regulating the timing of
159 pupariation.

160

161 **_brat_ restricts growth and proliferation during regeneration**

162 Regenerative growth occurs through localized cell proliferation at the wound site (Abbott
163 et al., 1981; Smith-Bolton et al., 2009).The proliferating cells, known as the blastema,
164 give rise to the regenerated tissue. The blastema and the subsequent regenerated wing
165 pouch can be labeled with the wing primordium marker Nubbin (Nub) (Ng et al., 1995).
166 To determine whether $brat^{1}$/+ discs regenerated better due to increased growth rates in
167 the wing pouch, we measured the area of the Nub-expressing cells in control and
168 $brat^{1}$/+ regenerating discs. In the initial stages of regeneration, the control and mutant
169 had similar Nub-expressing areas, indicating equal ablation and equal early regrowth.
170 However, by 48 hours after tissue damage (recovery time 48, or R48), $brat^{1}$/+ wing
171 discs had a significantly bigger Nub-expressing pouch than the control (Figure 2D-F),
172 indicating that *brat*/+ mutants were regenerating faster than controls. To assess whether
173 this difference in growth rates was due to differences in proliferation, we counted cells
174 going through mitosis by quantifying Phospho-histone H3 (PH3)-positive nuclei in the
175 regenerating blastema. Reduction of *brat* resulted in a significantly higher number of
176 PH3-positive nuclei per area at R0, but this increased proliferation had subsided to
177 normal levels by R24 (Figure 2G-I). To confirm that the increased number of PH3-
178 positive nuclei were not simply due to an increased number of total cells in the
179 blastema, we also counted total Nubbin-positive nuclei in the regenerating blastema to

calculate a ratio of proliferating cells to blastema cells (Figure S2C). These data confirm increased proliferation in *brat*^{1}/+ regenerating discs at R0. Differences in proliferation early in regeneration often become evident later when measuring wing pouch area (Brock et al., 2017). Therefore, reduction of *brat* gives the regenerating tissue a growth advantage early in regeneration, resulting in a measurable difference in tissue area by R48.

Wingless (Wg) and Myc are regulators of regenerative growth and are upregulated at the wound site after damage (McClure and Schubiger, 2008; Schubiger et al., 2010; Smith-Bolton et al., 2009). Interestingly, Brat regulates stem cell differentiation in the brain by suppressing self-renewal signaling pathways such as Wnt signaling, and acting as a post-transcriptional inhibitor of Myc, to enable specification of progenitor cell fate (Betschinger et al., 2006; Komori et al., 2014). Additionally, Brat overexpression can suppress Myc at the post-transcriptional level in wing disc epithelial cells, although loss of *brat* does not lead to elevated Myc protein in wing discs during normal development (Ferreira et al., 2014). To determine whether these regulators of regenerative growth are upregulated in *brat*^{1}/+ regenerating discs, we examined the expression of Wg and Myc. Wg is normally expressed along the Dorso-ventral (DV) boundary and in two concentric circles at the inner and outer edge of the wing pouch (Couso et al., 1993) (Figure 3A), and Myc is expressed in the wing pouch, but is repressed in the cells at the DV boundary as they undergo cell cycle and growth arrest (Wu and Johnston, 2010) (Figure 3B). Both Wg and Myc expression were comparable to controls in undamaged *brat*^{1}/+ discs (Figure S3A-E). When damage is induced, Wg is upregulated throughout

the blastema by R0 (Smith-Bolton et al., 2009) (Figure 3C). Reduction of *brat* expression resulted in significantly higher levels of Wg expression at R0 (Figure 3D and 3E) but not at R24 (Figure 3F). After ablation, Myc expression is elevated in the regenerating tissue (Smith-Bolton et al., 2009) (Figure 3G and 3H). $brat^{1}$/+ discs showed significantly higher levels of Myc at R0, which were sustained through R24 (Figure 3I-K). Thus, loss of *brat* caused an increase in the levels of both Wg and Myc early in regeneration. The elevated expression of these growth regulators likely explains the high proliferation seen in $brat^{1}$/+ discs at R0, and the larger wing pouch at R48.

brat **is required for margin cell-fate specification during regeneration**

Reduction of *brat* during regeneration caused patterning defects specifically at the wing margin, resulting in the loss of vein at the margin and loss of sensory bristles (Figure 1G). Thus, *brat* is required for correct cell-fate specification at the DV boundary during regeneration. The wing imaginal disc is divided into the dorsal and the ventral compartments, with expression of the LIM-homeodomain protein Apterous (Ap) in dorsal cells. The juxtaposition of the dorsal and ventral cells forms the DV boundary, which develops into the adult wing margin (Diaz-Benjumea and Cohen, 1993) (Figure 4A). Notch (N) and Wg signaling at the DV boundary are crucial for the correct organization and cell-fate specification at the boundary (Micchelli et al., 1997). *cut (ct)* and *achaete (ac)* are margin-specific genes that are expressed downstream of N and Wg signaling. *ct* is required for the specification of the wing margin, and *ac* specifies the

224 pro-neural sensory organ precursors (Becam and Milán, 2008; Micchelli et al., 1997)
225 (Figure 4A).

226

227 To investigate whether the errors in fate specification seen in *brat*^{1}/+ discs were due to
228 a compromised compartment boundary, we examined the expression of Ap using the
229 *ap-lacZ* reporter. *ap-lacZ* expression showed a clear DV boundary in the undamaged
230 control discs (Figure 4B). The DV boundary remained intact after ablation in control and
231 *brat*^{1}/+ discs (Figure 4C-D, Figure S4A and S4B). *ap-lacZ* expression was also seen in
232 the debris found in the damaged wing imaginal disc, due to the perdurance of β-gal. Wg
233 expression was restored to its normal DV expression by R48 in both control and *brat*^{1}/+
234 discs (Figure S4C and S4D). Therefore, the patterning defects were not caused by
235 disruptions in the DV boundary or changes in Wg expression.

236

237 Next, we examined N signaling in *brat*^{1}/+ discs due to its critical role in specifying fates
238 at the DV boundary. We used a N signaling reporter, which uses *Notch Response*
239 *Elements* (*NREs*) that bind to the Notch co-receptor Suppressor of Hairless, to drive the
240 expression of GFP (Saj et al., 2010). No difference was detected in the expression of
241 the N reporter for undamaged control and *brat*^{1}/+ discs (Figure 4E and 4F). N signaling
242 at the DV boundary was restored by R24 in controls and continued at R48 (Figure 4G
243 and 4H). Note that the reporter signal can also be seen in cellular debris in the
244 regenerating discs due to the perdurance of GFP. Interestingly, *brat*^{1}/+ discs showed
245 highly elevated levels of the N signaling reporter at both these time points (Figure 4I and

4J). This result is consistent with recent evidence demonstrating Brat's ability to attenuate N nuclear transport in the brain (Mukherjee et al., 2016). We wondered whether this elevated N signaling could also disrupt margin fates. However, overexpressing the N-intracellular domain in the wing pouch during the 24-hour ablation period (Figure S4E and S4F) resulted in adult wings that were patterned remarkably well, with significantly fewer wings showing any margin defects when compared to the control (Figure S4G). Thus, increased N activity during regeneration suppresses margin defects. Additionally, decreasing N signaling activity in *brat*^{1}/+ regenerating discs by using a mutation in the *anterior pharynx defective 1 (aph-1)* gene was unable to rescue the loss of *brat* phenotype. *aph-1*^{D35}/+ discs showed significantly reduced N signaling during normal development (Figure S4H-J) and at R24 during regeneration (Figure S4K-M), but could not rescue the loss of margin phenotype in the *brat* mutant (Figure S4N). Thus, while Brat constrains N signaling during regeneration, the elevated N signaling in *brat*^{1}/+ mutants does not cause the margin cell-fate specification defects.

brat **specifies margin fate by controlling the expression of Cut and Achaete**

To understand how patterning was disrupted in *brat*^{1}/+ regenerating discs, we examined expression of margin cell-fate genes. Cut (Ct) expression was present along the DV boundary in both undamaged control and *brat*^{1}/+ discs (Figure 4K and 4L), consistent with our results showing that adult undamaged *brat*^{1}/+ wings do not have margin defects (Figure S1D). In control regenerating discs, Ct expression was detected at the DV boundary at R72, which is when regeneration and repatterning are largely complete

(Figure 4M). By contrast, Ct expression was either not observed in *brat*^{1}/+ discs or was still missing in segments of the DV boundary at R72 (Figure 4N and 4O). These results indicate a specific error in cell-fate specification, as the DV boundary was intact at R72 (Figure S4A and S4B). Undamaged control and *brat*^{1}/+ discs also showed appropriate Ac expression in two stripes of cell directly flanking the DV boundary in the anterior half of the disc (Figure 4P and 4Q). Ac expression was also detected in control regenerating discs at R72 (Figure 4R). While Ac-expressing cells appeared in *brat*^{1}/+ discs, they were not clearly separated across the DV boundary (Figure 4S). This finding is consistent with previous reports showing that Ct suppresses Ac at the margin, and mutations in *ct* lead to aberrant expression of Ac at the DV boundary, followed by degeneration of the wing margin through cell death (Couso et al., 1994; Jack et al., 1991).

High Myc expression perturbs margin cell-fate specification during regeneration

Our results show that Brat both restricts regenerative growth and ensures correct cell-fate specification at the wing margin. Interestingly, JNK signaling in regenerating tissue can cause aberrant posterior-to-anterior cell-fate changes, which can be suppressed by a regeneration-specific protective factor, Taranis, to ensure correct patterning of the regenerating tissue (Schuster and Smith-Bolton, 2015). Therefore, we wondered whether unconstrained regenerative growth, or unconstrained expression of growth drivers, could also have deleterious side effects such as loss of margin cell fates. As Wg expression is normal during late regeneration and we have ruled out elevated N

290 signaling as the causative factor for the cell-fate errors that occurred in *brat*^{1}/+
291 regenerating discs, we wondered whether high Myc levels caused by reduced Brat
292 could cause the margin defects.

293

294 Brat overexpression can suppress Myc in wing imaginal disc cells (Ferreira et al., 2014),
295 and in undamaged wing discs Brat protein levels were elevated at the DV boundary
296 where Myc was reduced (Figure 5A and 5A'), suggesting that Brat may regulate Myc at
297 the DV boundary. Furthermore, our results showed that regenerating *brat*/+ mutant
298 discs experienced elevated Myc levels compared to controls (Figure 3G-K). Previous
299 studies demonstrated that Brat regulates Myc at the post-transcriptional level (Ferreira
300 et al., 2014). To confirm that Brat is also regulating *myc* post-transcriptionally during
301 regeneration, we measured *myc* transcript levels through qPCR. Regenerating discs
302 showed significantly increased transcription of *myc* compared to undamaged controls.
303 However, there was no significant difference in *myc* transcript levels between
304 regenerating control and *brat*^{1}/+ discs at R0 and R24 (Figure 5B and 5C), indicating that
305 Brat's regulation of Myc must be post-transcriptional.

306

307 To test whether the elevated Myc protein levels could cause margin defects during
308 regeneration and phenocopy the *brat* mutation, we overexpressed Myc in the wing
309 pouch during the 24-hour ablation period. Myc was highly upregulated at R0 (Figure 5D-
310 F), but Myc levels had returned to normal by R24 (Figure 5F). Overexpression of Myc
311 also resulted in a significantly higher number of proliferating nuclei in the regenerating

312 tissue at R0, similar to *brat*^{1}/+ discs (Figure 5G-I). Remarkably, we observed that adult
313 wings resulting from Myc-overexpressing regenerating discs also showed margin
314 defects similar to the *brat*^{1}/+ wings (Figure 5J and 5K). Moreover, the frequency of
315 margin defects in the adult wings resulting from Myc-overexpressing regenerating discs
316 was even higher than in adult wings resulting from *brat*^{1}/+ regenerating discs (Figure
317 5L), demonstrating that elevated levels of Myc alone can cause errors in margin cell-
318 fate specification. Similar to *brat*^{1}/+ discs, *ap-lacZ* expression showed that the
319 compartment boundary was not compromised in Myc-overexpressing regenerating
320 discs (Figure 5M and 5N). Likewise, Ct expression was missing in segments at the DV
321 boundary as in the *brat*^{1}/+ discs (Figure 5O and 5P).

322

323 Overexpressing Myc for a 24-hour window during normal development resulted in 3
324 adult wings out of 730 that showed any margin defects (Figure S5A). Even in these
325 wings, only one segment of the margin was affected. To rule out the possibility that
326 transient overexpression of Myc during development may not be sufficient to perturb
327 patterning, we overexpressed Myc continuously after the animals entered the third
328 instar larval stage. Continuous Myc overexpression proved to be lethal for many
329 animals. While the flies that survived had significantly smaller wings, the margins
330 showed no defect (Figure 5Q and 5R). 31 hours of Myc overexpression during normal
331 development showed significantly higher Myc protein levels (Figure 5S-U) but did not
332 interfere with Ct expression (Figure 5V and 5W). These data indicate that high Myc
333 levels do not cause cell-fate specification errors during normal development, and the

334 extensive loss of wing margin induced by high Myc expression is a regeneration-specific
335 phenotype.

336

337 We hypothesized that if the *brat* phenotype was due to elevated Myc levels, we would
338 be able to rescue the phenotype by reducing Myc levels in the *brat* mutant. For this
339 purpose, we used dm^4, which is a null allele of Myc (Pierce et al., 2004). Surprisingly,
340 we observed that the dm^4/+ mutants alone showed margin defects in the regenerated
341 wings at a frequency similar to $brat^1$/+, even though the dm^4/+; $brat^1$/+ double mutant
342 showed slightly reduced frequency of margin defects (Figure S5B). To confirm that Myc
343 levels were reduced in the dm^4/+ mutants, we quantified Myc protein through
344 immunostaining. We observed that there was no significant difference in Myc
345 expression levels between the dm^4/+ mutant and control, both during development and
346 regeneration (Figure S5C and S5D). Indeed, Myc levels were trending higher in the
347 dm^4/+ discs during regeneration. The failure of the dm^4 mutation to reduce Myc levels
348 could be due to compensatory expression of the functional copy of the Myc locus. We
349 next tried reducing Myc levels though RNAi. Despite the RNAi expression being
350 transient in our system, and only occurring in cells that survive ablation, RNAi-mediated
351 persistent knockdown has worked for multiple genes, likely due to the shadow RNAi
352 effect (Bosch et al., 2016). Two RNAi lines could significantly reduce Myc levels during
353 normal development when expressed during early third instar (Figure S5E). However,
354 when Myc RNAi was expressed during the 24-hour ablation period, Myc levels were not
355 reduced at either R0 or R24, with one Myc RNAi line showing significantly higher levels
356 of Myc compared to the control (Figure S5F). Thus, compensatory regulation of Myc

357 expression during regeneration prevented us from testing whether reduction in Myc
358 could rescue the *brat/+* phenotype.

359

360 Interestingly, animals that overexpressed Myc in the wing pouch during ablation did not
361 undergo a regeneration-induced pupariation delay (Figure S5G), suggesting that Brat
362 regulates the entry into metamorphosis independently of its regulation of Myc.
363 Therefore, not all effects of loss of Brat are mediated through Myc.

364

365 **Enhanced proliferation does not disrupt margin cell-fate specification during**
366 **regeneration**

367 Myc is an important driver of regenerative growth, and yet, we found that cell-fate
368 specification during regeneration can be negatively affected if Myc levels are not
369 constrained. To test whether the aberrant patterning was a specific result of high Myc
370 levels or whether increases in growth and proliferation could, in general, cause margin
371 defects, we also increased proliferation during regeneration by overexpressing both
372 *cyclinE (cycE)* and *string (stg)*.

373

374 Overexpressing the cell cycle genes in the wing imaginal disc during the 24-hour
375 ablation period caused the resulting adult wings to be much larger than controls that
376 had also undergone damage and regeneration (Figure 6A), though not larger than a
377 normal wing. No significant regeneration-induced pupariation delay was seen, making

the enhanced regeneration even more remarkable (Figure 6B). Intriguingly, we did not observe many margin defects for wings that had experienced *cycE* and *stg* overexpression during regeneration (Figure 6C-E). Thus, pattern disruption during regeneration appears to be specifically associated with Myc overexpression and does not appear to be caused by increased proliferation alone.

Loss of cell-fate specification may be due to elevated expression of Chinmo

Given that driving growth by overexpressing Cyclin E and String does not cause loss of wing margin cell fates in regenerating tissue, this phenotype might be caused by misregulation of one or more targets of the Myc transcription factor. We have previously identified the gene *Chronologically inappropriate morphogenesis (chinmo)* as a novel regulator of regeneration (Khan et al., 2017). Chinmo is a transcription factor that regulates the balance between a proliferative self-renewal state and a differentiated state in stem cells (Dillard et al., 2017; Flaherty et al., 2010). Recent work has shown that *chinmo* also maintains wing epithelial cells in an unspecified state during development by inhibiting *ct* expression, and enhances regenerative potential (Narbonne-Reveau and Maurange, 2019). While *chinmo* mRNA can be a direct Brat target (Loedige et al., 2015), *chinmo* is regulated at the level of transcription in the wing imaginal disc (Narbonne-Reveau and Maurange, 2019). Therefore, we wondered whether *chinmo* could be misregulated downstream of Myc in the $brat^{1}$/+ regenerating discs. Interestingly, the model organism Encyclopedia of Regulatory Networks (modERN) data show Myc binding near the *chinmo* promoter, supporting this

hypothesis (Kudron et al., 2017). Chinmo levels were not significantly different in undamaged control and *brat*^{1}/+ discs (Figure 7A, 7B and 7E). However, Chinmo levels were significantly higher in *brat*^{1}/+ regenerating discs compared to control regenerating discs at R24 (Figure 7C, 7D and 7F). Thus, the loss of *ct* expression and loss of margin cell fates in *brat/+* regenerating discs may be due, at least in part, to upregulation of *chinmo*.

To confirm regulation of *chinmo* downstream of Myc, we examined Chinmo levels in regenerating discs over-expressing Myc. Chinmo levels were elevated in Myc-overexpressing discs at R0, when Myc overexpression was the highest (Figure 5F and Figure 7G-I). However, Chinmo levels were restored to control levels by R24 in Myc-overexpressing discs, consistent with the return of Myc levels to normal at this time point (Figure 5F and Figure S6A-C). Interestingly, Myc and Chinmo expression almost perfectly co-localized, consistent with the hypothesis that Myc regulates Chinmo expression (Figure S6A-B'''). Additionally, we observed a high correlation between Myc and Chinmo expression levels in individual discs (Figure S6D and S6E). Undamaged discs overexpressing Myc did not show elevated Chinmo levels (Figure S6F-H), possibly explaining why Myc overexpression during normal development did not cause margin defects. Importantly, other unidentified Myc targets may also contribute to *ct* misregulation in regenerating discs with reduced Brat or overexpressed Myc.

Based on our findings, we propose a model in which pro-growth factors are important for coordinating regenerative growth, but can lead to deleterious side effects by perturbing cell-fate gene expression and patterning. Brat prevents a prolonged proliferative and unspecified state in regenerating wing discs by inhibiting Wg, Ilp8, Myc and Chinmo to enable cessation of growth, induction of cell-fate specification, and entry into metamorphosis (Figure 8).

Discussion

Here we have shown that Brat acts as a protective factor during regeneration by constraining levels of transcription factors such as Myc and Chinmo, which promote growth and proliferation but also inhibit cell-fate specification. If Brat is unable to perform its protective function during regeneration, Myc levels increase unchecked, resulting in misregulation of its targets, including Chinmo and subsequently Ct, causing loss of proper cell fates at the wing margin.

Myc is broadly used across organisms to promote proliferation and prevent differentiation (Amati and Land, 1994; Takahashi and Yamanaka, 2006), and Myc is strongly activated in the regenerating wing imaginal discs and is required for efficient regeneration. Importantly, increased Myc levels can enhance regeneration in both younger discs as well as mature discs that normally regenerate poorly (Harris et al., 2016; Smith-Bolton et al., 2009). Nevertheless, we have found that while these abnormally high Myc levels can enhance regenerative growth, they also perturb

443 differentiation by misregulating target genes such as Chinmo. Thus, enhanced
444 regeneration happens at the expense of correct cell-fate specification.

445

446 Brat promotes differentiation in *Drosophila* larval neuroblasts and ovarian germline stem
447 cells by asymmetrically segregating to one of the daughter cells where it post-
448 transcriptionally inhibits Myc (Betschinger et al., 2006; Harris et al., 2011). This
449 daughter cell is then able to differentiate while the other daughter cell remains a stem
450 cell. In *brat* mutants, progeny of stem cells are unable to differentiate, resulting in an
451 abnormal expansion of the stem-cell population, which can form tumors in the brain
452 (Arama et al., 2000; Betschinger et al., 2006; Harris et al., 2011; Lee et al., 2006). Thus,
453 Brat protects these tissues from overproliferation of stem cells. Importantly, wing
454 imaginal disc regeneration is not stem-cell based, but in wing disc regeneration Brat
455 also inhibits Myc to allow correct cell-fate specification. Based on these similarities in
456 function, Brat likely acts as a protective factor across different biological contexts,
457 including regeneration that does not employ stem cells.

458

459 We have previously shown that JNK signaling can induce posterior-to-anterior fate
460 changes in regenerating wing discs, which can be prevented by the protective factor
461 Taranis (Schuster and Smith-Bolton, 2015). We have now identified a second protective
462 factor, Brat, which is needed specifically for correct patterning of the regenerating wing
463 margin. Interestingly, while elevated JNK signaling causes anterior markers to appear in
464 the posterior wing compartment, it does not cause margin loss, indicating that posterior

fate and margin fate are regulated in distinct ways (Schuster and Smith-Bolton, 2015). Protective factors such as Tara and Brat are important for maintaining the balance between fate specification and regenerative potential, but they do so by using very different mechanisms. While the molecular function of Tara is unknown, genetic interactions in *Drosophila* coupled with the demonstrated functions of its vertebrate homologs suggest it regulates gene expression at the level of transcription and chromatin (Calgaro et al., 2002; Hayashi et al., 2006; Hsu et al., 2001; Watanabe-Fukunaga et al., 2005). By contrast, Brat acts as a translational repressor, and suppresses its targets through mRNA degradation (Komori et al., 2018; Laver et al., 2015). Tara is required to prevent fate changes induced by JNK signaling, which is necessary for wound repair and regeneration but is not required for the normal development of the wing. By contrast, Myc is required for both development and regeneration of the wing disc, but is constrained by Brat only during regeneration.

An important open question in the field of regeneration is how patterning and cell-fate specification are regulated in regenerating tissue, and whether these mechanisms are different from the developmental program. Many studies have highlighted that regeneration must be distinct from development in some ways, because the damaged tissue already has complex patterning, and the wound-healing response causes strong activation of signaling pathways, some of which are not normally present in developing tissue (Bosch et al., 2010, 2005; Harris et al., 2016; Luttrell et al., 2016; McCusker and Gardiner, 2013; Myohara, 2004; Schuster and Smith-Bolton, 2015; Sun and Irvine, 2014; Vizcaya-Molina et al., 2018). We are just beginning to identify regulators like Brat

that are crucial for attenuating regenerative growth signaling and shielding the regenerating tissue from the harmful side effects of such signaling. Identification of these regulators highlights the fact that the regenerating tissue is distinct from normally developing tissue. Since regeneration signaling is complex and comprised of many signaling pathways, additional factors that play protective roles during regeneration likely exist. Identification of these factors will be important for the development of clinical therapies targeted at tissue repair, enabling these therapies to protect against the deleterious side effects of exogenous and unconstrained pro-growth signaling.

Materials and Methods

Ablation and Regeneration experiments

Ablation experiments were done as previously described (Schuster and Smith-Bolton, 2015). Briefly, cell death was induced by driving *UAS-reaper* under *rotund-GAL4*, with *GAL80^{ts}* for temporal control. Animals were raised at 18°C for 7 days after egg lay (AEL) (early third instar) before they were shifted to a 30°C circulating water bath for 24 hours. Animals were brought back to 18°C to allow regeneration. Wing discs were dissected at different time points after the end of ablation, or the animals were allowed to grow to adulthood to observe the adult wing phenotype. Undamaged control wing discs were the same genotype as the experimental animals but kept at 18°C and dissected on day 9 after egg lay, which is mid-late third instar. For undamaged adult wings, the animals were kept at 18°C until after eclosion. Any other undamaged conditions used are mentioned specifically in the figure legends.

Fly stocks

The following *Drosophila* stocks were used: w^{1118} (wild type)(Hazelrigg et al., 1984), w^{1118} *; rnGAL4, UAS-rpr, tubGAL80ts/TM6B,tubGAL80* (Smith-Bolton et al., 2009), $brat^{1}$ (Wright et al., 1976)(FBst0003988), $brat^{192}$ and $brat^{150}$ (Luschnig et al., 2004)(a gift from Juergen Knoblich, Austrain Academy of Science), $brat^{11}$ (Wright et al., 1981)(a gift from Chen-Yu Lee, University of Michigan), *Df(2L)Exel8040* (Parks et al., 2004)(FBst0007847), *Df(2L)TE37C-7* (Stathakis et al., 1995)(FBst0006089), *rnGAL4, tubGAL80ts/TM6B* (Smith-Bolton et al., 2009), *P{Trip.HM05078}attP2* (called *bratRNAi* in the text)(FBst0028590), *P{CaryP}attP2* (called *attP2* control in the text)(FBst0036303), *{PZ}*ap^{rK568} (Cohen et al., 1992)(FBst0005374), *NRE-GFP* (Saj et al., 2010)(FBst0030727), *UAS-Nintra* (a gift from Gary Struhl, Columbia University), $aph\text{-}1^{D35}$ (Littleton and Bellen, 1994)(FBst0063242), *UAS-Myc* (Johnston et al., 1999) (FBst0009674), *UAS-cycE, stg* (a gift from Laura Buttitta, University of Michigan), dm^{4} (Pierce et al., 2004), *P{GD1419}v2947* (called *MycRNAi#1* in the text)(VDRC ID# 2947) and *P{GD1419}v2948* (called *MycRNAi#2* in the text)(VDRC ID# 2948), *P{GD6000}v15293* (called control in the text) (VDRC ID# 15293)(93). All fly stocks are available from the Bloomington Drosophila Stock Center unless stated otherwise.

Pupariation timing

Pupariation experiments were performed in a similar manner to the ablation experiments. Starting at day 9, newly formed pupal cases were counted in each vial.

Pupal cases were counted every 24 hours, up until day 15. Pupariation rates from three independent experiments were used to calculate the average plotted in the graphs.

Immunohistochemistry

Immunostaining was carried out as previously described (Smith-Bolton et al., 2009). Primary antibodies were rat anti-Brat (1:200) (Sonoda and Wharton, 2001) (a gift from Robin Wharton, Ohio State University), mouse anti-Nubbin (1:500) (Averof and Cohen, 1997) (a gift from Steve Cohen, University of Copenhagen), rabbit anti-Phospho-Histone H3 (1:500) (Millipore), mouse anti-Wingless (1:100) (The Developmental Studies Hybridoma Bank [DSHB]), rabbit anti-dMyc (1:500) (Santa Cruz Biotechnologies), mouse anti-βgal (1:100) (DSHB), mouse anti-Cut (1:10) (DSHB), mouse anti-Achaete (1:10)(DSHB), rat anti-Chinmo (1:500) (a gift from Nick Sokol, Indiana University). The Developmental Studies Hybridoma Bank (DSHB) was created by the NICHD of the NIH and is maintained at the University of Iowa, Department of Biology, Iowa City, IA 52242.

Secondary antibodies were AlexaFluor probes (1:1000) (Life Technologies). DNA was marked using TO-PRO3 (1:500) (Life Technologies) or DAPI (1:5000 of 0.5 mg/mL stock) (Sigma). Discs were mounted in Vectashield mounting medium (Vector Laboratories).

553 Discs were imaged on a Zeiss LSM 510 or a Zeiss LSM 700 confocal microscope.
554 Parameters for imaging were identical for quantified images. Images were processed
555 using ZEN lite (Zeiss), ImageJ (NIH) and Photoshop (Adobe). Maximum intensity
556 projections were created for the confocal images. Fluorescence intensity was measured
557 within the wing pouch as marked by anti-Nubbin or by using the morphology of the
558 undamaged wing disc. Myc and Chinmo intensities were measure by outlining the
559 region expressing elevated Myc or Chinmo levels. *NRE-GFP* intensity was measured by
560 outlining the GFP-expressing region at the DV boundary.

561

562 **Adult wing quantifications**

563 Adult wings were mounted in Gary's Magic Mount (Canada balsam [Sigma] dissolved in
564 methyl salicylate [Sigma]). Images were taken with an Olympus SZX10 microscope with
565 an Olympus DP21 camera using the CellSens Dimension software (Olympus).

566

567 All adult wings that were 75% or 100% the size of a normal wing were used to quantify
568 the loss of the wing margin. The wing margin was divided into five segments defined by
569 where the wing veins intersect the margin. Each wing was scored for the number of
570 segments with missing margin to assess the extent of the patterning defect.
571 Percentages from the three independent experiments were used to calculate averages
572 plotted in the graphs. The area of undamaged and regenerated wings was measured
573 using ImageJ (NIH). ImageJ was also used to measure the percentage of linear length
574 of margin lost for the entire perimeter of the wing. Graphs were plotted using Excel and
575 Graphpad Prism 7.

576

577 **qPCR**

578 For quantitative PCR (qPCR), 40-60 wing imaginal discs were collected in Schneider's
579 medium and stored at -80°C. RNA was extracted using the Qiagen RNeasy Mini Kit
580 (#74104), and cDNA synthesis was performed using the Superscript III First Strand
581 Synthesis kit (#11752-050). qPCR reactions using the Power SYBR Green MasterMix
582 (ABI) were run on the ABI Step One Plus Real Time PCR System. The experiment
583 consisted of 3 biological replicates. For each biological replicate there were three
584 technical replicates. Gene expression was analyzed by the $\Delta\Delta C_t$ method and
585 normalized to *Gapdh2* expression. The following primers were used: *Gapdh2* forward
586 primer (GTGAAGCTGATCTCTTGGTACGAC), *Gapdh2* reverse primer
587 (CCGCGCCCTAATCTTTAACTTTTAC) (Classen et al., 2009), *ilp8* primers used from
588 Qiagen (QT00510552), *dmyc* forward primer (AACGATATGGTGGACGATGG), and
589 *dmyc* reverse primer (CGGCAGATTGAAGTTATTGTAGC) (Mitchell et al., 2010). For
590 qPCR experiments undamaged controls were *rnGAL4, tubGAL80ts/TM6B* females
591 crossed to w^{1118} males and shifted to 30˚C for 24 hours at 7 days AEL. Discs were
592 dissected either immediately or 24 hours after shifting the animals back to 18˚C for R0
593 and R24 time points, respectively.

594

595 **Acknowledgements**

596 The authors would like to thank Amanda Brock and Sumbul Khan for critical reading of
597 the manuscript and helpful discussions; Juergen Knoblich, Cheng-Yu Lee, Gary Struhl,

Robin Wharton, Nick Sokol, Laura Buttitta, the Bloomington Drosophila Stock Center (NIH P40OD018537), Vienna Drosophila Resource Center and the Developmental Studies Hybridoma Bank for reagents.

Author Contribution Section

Experiments were designed by SNFA and RKSB, and conducted and analyzed by SNFA. The manuscript was written by SNFA and RKSB.

Competing interests

The authors declare no competing interests.

References

Abbott LC, Karpen GH, Schubiger G. 1981. Compartmental restrictions and blastema formation during pattern regulation in Drosophila imaginal leg discs. *Dev Biol* **87**:64–75. doi:10.1016/0012-1606(81)90061-0

Amati B, Land H. 1994. Myc—Max—Mad: a transcription factor network controlling cell cycle progression, differentiation and death. *Curr Opin Genet Dev* **4**:102–108. doi:10.1016/0959-437x(94)90098-1

Arama E, Dickman D, Kimchie Z, Shearn A, Lev Z. 2000. Mutations in the β-propeller

620 domain of the Drosophila brain tumor (brat) protein induce neoplasm in the larval brain.
621 *Oncogene* **19**:1203706. doi:10.1038/sj.onc.1203706
622
623 Averof M, Cohen SM. 1997. Evolutionary origin of insect wings from ancestral gills.
624 *Nature* **385**:385627a0. doi:10.1038/385627a0
625
626 Bando T, Ishimaru Y, Kida T, Hamada Y, Matsuoka Y, Nakamura T, Ohuchi H, Noji S,
627 Mito T. 2013. Analysis of RNA-Seq data reveals involvement of JAK/STAT signalling
628 during leg regeneration in the cricket Gryllus bimaculatus. *Development* **140**:959–964.
629 doi:10.1242/dev.084590
630
631 Bando T, Mito T, Maeda Y, Nakamura T, Ito F, Watanabe T, Ohuchi H, Noji S. 2009.
632 Regulation of leg size and shape by the Dachsous/Fat signalling pathway during
633 regeneration. *Development* **136**:2235–2245. doi:10.1242/dev.035204
634
635 Becam I, Milán M. 2008. A permissive role of Notch in maintaining the DV affinity
636 boundary of the Drosophila wing. *Dev Biol* **322**:190–198.
637 doi:10.1016/j.ydbio.2008.07.028
638
639 Bergantiños C, Corominas M, Serras F. 2010. Cell death-induced regeneration in wing
640 imaginal discs requires JNK signalling. *Development* **137**:1169–1179.
641 doi:10.1242/dev.045559
642

643 Betschinger J, Mechtler K, Knoblich JA. 2006. Asymmetric Segregation of the Tumor
644 Suppressor Brat Regulates Self-Renewal in Drosophila Neural Stem Cells. *Cell*
645 **124**:1241–1253. doi:10.1016/j.cell.2006.01.038
646
647 Bosch JA, Sumabat TM, Hariharan IK. 2016. Persistence of RNAi-Mediated Knockdown
648 in Drosophila Complicates Mosaic Analysis Yet Enables Highly Sensitive Lineage
649 Tracing. *Genetics* **203**:109–118. doi:10.1534/genetics.116.187062
650
651 Bosch M, Bishop S-A, Baguña J, Couso J-P. 2010. Leg regeneration in Drosophila
652 abridges the normal developmental program. *Int J Dev Biol* **54**:1241–1250.
653 doi:10.1387/ijdb.093010mb
654
655 Bosch M, Serras F, Martín-Blanco E, Baguñà J. 2005. JNK signaling pathway required
656 for wound healing in regenerating Drosophila wing imaginal discs. *Dev Biol* **280**:73–86.
657 doi:10.1016/j.ydbio.2005.01.002
658
659 Brock AR, Seto M, Smith-Bolton RK. 2017. Cap-n-Collar Promotes Tissue Regeneration
660 by Regulating ROS and JNK Signaling in the Drosophila melanogaster Wing Imaginal
661 Disc. *Genetics* **206**:1505–1520. doi:10.1534/genetics.116.196832
662
663 Calgaro S, Boube M, Cribbs DL, Bourbon H-M. 2002. The Drosophila gene taranis
664 encodes a novel trithorax group member potentially linked to the cell cycle regulatory
665 apparatus. *Genetics* **160**:547–60.

Chen G, Kong J, Tucker-Burden C, Anand M, Rong Y, Rahman F, Moreno CS, Meir EG, Hadjipanayis CG, Brat DJ. 2014. Human Brat Ortholog TRIM3 Is a Tumor Suppressor That Regulates Asymmetric Cell Division in Glioblastoma. *Cancer Res* **74**:4536–4548. doi:10.1158/0008-5472.can-13-3703

Classen A-K, Bunker BD, Harvey KF, Vaccari T, Bilder D. 2009. A tumor suppressor activity of Drosophila Polycomb genes mediated by JAK-STAT signaling. *Nat Genet* **41**:1150–1155. doi:10.1038/ng.445

Cohen B, McGuffin M, Pfeifle C, Segal D, Cohen S. 1992. apterous, a gene required for imaginal disc development in Drosophila encodes a member of the LIM family of developmental regulatory proteins. *Gene Dev* **6**:715–729. doi:10.1101/gad.6.5.715

Colombani J, Andersen DS, Léopold P. 2012. Secreted Peptide Dilp8 Coordinates *Drosophila* Tissue Growth with Developmental Timing. *Science* **336**:582–585. doi:10.1126/science.1216689

Couso J, Bate M, Martinez-Arias A. 1993. A wingless-dependent polar coordinate system in Drosophila imaginal discs. *Science* **259**:484–489. doi:10.1126/science.8424170

Couso J, Bishop S, Arias MA. 1994. The wingless signalling pathway and the patterning

689 of the wing margin in Drosophila. *Dev Camb Engl* **120**:621–36.

690

691 Diaz-Benjumea FJ, Cohen SM. 1993. Interaction between dorsal and ventral cells in the

692 imaginal disc directs wing development in Drosophila. *Cell* **75**:741–752.

693 doi:10.1016/0092-8674(93)90494-b

694

695 Dillard C, Narbonne-Reveau K, Foppolo S, Lanet E, Maurange C. 2017. Two distinct

696 mechanisms silence chinmo in Drosophila neuroblasts and neuroepithelial cells to limit

697 their self-renewal. *Development* **145**:dev.154534. doi:10.1242/dev.154534

698

699 Fan Y, Wang S, Hernandez J, Yenigun V, Hertlein G, Fogarty CE, Lindblad JL,

700 Bergmann A. 2014. Genetic Models of Apoptosis-Induced Proliferation Decipher

701 Activation of JNK and Identify a Requirement of EGFR Signaling for Tissue

702 Regenerative Responses in Drosophila. *Plos Genet* **10**:e1004131.

703 doi:10.1371/journal.pgen.1004131

704

705 Ferreira A, Boulan L, Perez L, Milán M. 2014. Mei-P26 Mediates Tissue-Specific

706 Responses to the Brat Tumor Suppressor and the dMyc Proto-Oncogene in Drosophila.

707 *Genetics* **198**:249–258. doi:10.1534/genetics.114.167502

708

709 Flaherty M, Salis P, Evans CJ, Ekas LA, Marouf A, Zavadil J, Banerjee U, Bach EA.

710 2010. chinmo Is a Functional Effector of the JAK/STAT Pathway that Regulates Eye

711 Development, Tumor Formation, and Stem Cell Self-Renewal in Drosophila. *Dev Cell*

712 **18**:556–568. doi:10.1016/j.devcel.2010.02.006

713

714 Garelli A, Gontijo AM, Miguela V, Caparros E, Dominguez M. 2012. Imaginal Discs
715 Secrete Insulin-Like Peptide 8 to Mediate Plasticity of Growth and Maturation. *Science*
716 **336**:579–582. doi:10.1126/science.1216735

717

718 Grijalva JL, Huizenga M, Mueller K, Rodriguez S, Brazzo J, Camargo F, Sadri-Vakili G,
719 Vakili K. 2014. Dynamic alterations in Hippo signaling pathway and YAP activation
720 during liver regeneration. *Am J Physiol-gastr L* **307**:G196–G204.
721 doi:10.1152/ajpgi.00077.2014

722

723 Grusche FA, Degoutin JL, Richardson HE, Harvey KF. 2011. The Salvador/Warts/Hippo
724 pathway controls regenerative tissue growth in Drosophila melanogaster. *Dev Biol*
725 **350**:255–266. doi:10.1016/j.ydbio.2010.11.020

726

727 Gupta V, Gemberling M, Karra R, Rosenfeld GE, Evans T, Poss KD. 2013. An Injury-
728 Responsive Gata4 Program Shapes the Zebrafish Cardiac Ventricle. *Curr Biol* **23**:1221–
729 1227. doi:10.1016/j.cub.2013.05.028

730

731 Halme A, Cheng M, Hariharan IK. 2010. Retinoids Regulate a Developmental
732 Checkpoint for Tissue Regeneration in Drosophila. *Curr Biol* **20**:458–463.
733 doi:10.1016/j.cub.2010.01.038

734

735 Hanovice NJ, Leach LL, Slater K, Gabriel AE, Romanovicz D, Shao E, Collery R, Burton
736 EA, Lathrop KL, Link BA, Gross JM. 2019. Regeneration of the zebrafish retinal pigment
737 epithelium after widespread genetic ablation. *Plos Genet* **15**:e1007939.
738 doi:10.1371/journal.pgen.1007939
739
740 Hariharan IK, Serras F. 2017. Imaginal disc regeneration takes flight. *Curr Opin Cell Biol*
741 **48**:10–16. doi:10.1016/j.ceb.2017.03.005
742
743 Harris RE, Pargett M, Sutcliffe C, Umulis D, Ashe HL. 2011. Brat Promotes Stem Cell
744 Differentiation via Control of a Bistable Switch that Restricts BMP Signaling. *Dev Cell*
745 **20**:72–83. doi:10.1016/j.devcel.2010.11.019
746
747 Harris RE, Setiawan L, Saul J, Hariharan IK. 2016. Localized epigenetic silencing of a
748 damage-activated WNT enhancer limits regeneration in mature Drosophila imaginal
749 discs. *Elife* **5**:e11588. doi:10.7554/elife.11588
750
751 Hayashi R, Goto Y, Ikeda R, Yokoyama KK, Yoshida K. 2006. CDCA4 Is an E2F
752 Transcription Factor Family-induced Nuclear Factor That Regulates E2F-dependent
753 Transcriptional Activation and Cell Proliferation. *J Biol Chem* **281**:35633–35648.
754 doi:10.1074/jbc.m603800200
755
756 Hayashi S, Ochi H, Ogino H, Kawasumi A, Kamei Y, Tamura K, Yokoyama H. 2014.
757 Transcriptional regulators in the Hippo signaling pathway control organ growth in

758 Xenopus tadpole tail regeneration. *Dev Biol* **396**:31–41.
759 doi:10.1016/j.ydbio.2014.09.018
760
761 Hazelrigg T, Levis R, Rubin GM. 1984. Transformation of white locus DNA in
762 Drosophila: Dosage compensation, zeste interaction, and position effects. *Cell* **36**:469–
763 481. doi:10.1016/0092-8674(84)90240-x
764
765 Hobmayer B, Rentzsch F, Kuhn K, Happel CM, von Laue C, Snyder P, Rothbächer U,
766 Holstein TW. 2000. WNT signalling molecules act in axis formation in the diploblastic
767 metazoan Hydra. *Nature* **407**:186. doi:10.1038/35025063
768
769 Hsu S, Yang C, Sim K, Hentschel DM, O'Leary E, Bonventre JV. 2001. TRIP-Br: a novel
770 family of PHD zinc finger- and bromodomain-interacting proteins that regulate the
771 transcriptional activity of E2F-1/DP-1. *Embo J* **20**:2273–2285.
772 doi:10.1093/emboj/20.9.2273
773
774 Jack J, Dorsett D, Delotto Y, Liu S. 1991. Expression of the cut locus in the Drosophila
775 wing margin is required for cell type specification and is regulated by a distant
776 enhancer. *Dev Camb Engl* **113**:735–47.
777
778 Jiang H, Grenley MO, Bravo M-J, Blumhagen RZ, Edgar BA. 2011. EGFR/Ras/MAPK
779 Signaling Mediates Adult Midgut Epithelial Homeostasis and Regeneration in
780 Drosophila. *Cell Stem Cell* **8**:84–95. doi:10.1016/j.stem.2010.11.026

781

782 Jin Y, Ha N, Forés M, Xiang J, Gläßer C, Maldera J, Jiménez G, Edgar BA. 2015.
783 EGFR/Ras Signaling Controls Drosophila Intestinal Stem Cell Proliferation via Capicua-
784 Regulated Genes. *Plos Genet* **11**:e1005634. doi:10.1371/journal.pgen.1005634

785

786 Johnston LA, Prober DA, Edgar BA, Eisenman RN, Gallant P. 1999. Drosophila myc
787 Regulates Cellular Growth during Development. *Cell* **98**:779–790. doi:10.1016/s0092-
788 8674(00)81512-3

789

790 Katsuyama T, Comoglio F, Seimiya M, Cabuy E, Paro R. 2015. During Drosophila disc
791 regeneration, JAK/STAT coordinates cell proliferation with Dilp8-mediated
792 developmental delay. *Proc National Acad Sci* **112**:E2327–E2336.
793 doi:10.1073/pnas.1423074112

794

795 Kawakami Y, Esteban C, Raya M, Kawakami H, Martí M, Dubova I, Belmonte J. 2006.
796 Wnt/β-catenin signaling regulates vertebrate limb regeneration. *Gene Dev* **20**:3232–
797 3237. doi:10.1101/gad.1475106

798

799 Khan S, Abidi S, Skinner A, Tian Y, Smith-Bolton RK. 2017. The Drosophila Duox
800 maturation factor is a key component of a positive feedback loop that sustains
801 regeneration signaling. *Plos Genet* **13**:e1006937. doi:10.1371/journal.pgen.1006937

802

803 Komori H, Golden KL, Kobayashi T, Kageyama R, Lee C-Y. 2018. Multilayered gene

804 control drives timely exit from the stem cell state in uncommitted progenitors during
805 Drosophila asymmetric neural stem cell division. *Gene Dev* **32**:1550–1561.
806 doi:10.1101/gad.320333.118
807
808 Komori H, Xiao Q, McCartney BM, Lee C-Y. 2014. Brain tumor specifies intermediate
809 progenitor cell identity by attenuating β-catenin/Armadillo activity. *Development* **141**:51–
810 62. doi:10.1242/dev.099382
811
812 Kudron MM, Victorsen A, Gevirtzman L, Hillier LW, Fisher WW, Vafeados D, Kirkey M,
813 Hammonds AS, Gersch J, Ammouri H, Wall ML, Moran J, Steffen D, Szynkarek M,
814 Seabrook-Sturgis S, Jameel N, Kadaba M, Patton J, Terrell R, Corson M, Durham TJ,
815 Park S, Samanta S, Han M, Xu J, Yan K-K, Celniker SE, White KP, Ma L, Gerstein M,
816 Reinke V, Waterston R. 2017. The modERN Resource: Genome-Wide Binding Profiles
817 for Hundreds of Drosophila and Caenorhabditis elegans Transcription Factors. *Genetics*
818 **208**:genetics.300657.2017. doi:10.1534/genetics.117.300657
819
820 Kudryashova E, Kramerova I, Spencer MJ. 2012. Satellite cell senescence underlies
821 myopathy in a mouse model of limb-girdle muscular dystrophy 2H. *J Clin Invest*
822 **122**:1764–1776. doi:10.1172/jci59581
823
824 Laver JD, Li X, Ray D, Cook KB, Hahn NA, Nabeel-Shah S, Kekis M, Luo H, Marsolais
825 AJ, Fung KY, Hughes TR, Westwood TJ, Sidhu SS, Morris Q, Lipshitz HD, Smibert CA.
826 2015. Brain tumor is a sequence-specific RNA-binding protein that directs maternal

827 mRNA clearance during the Drosophila maternal-to-zygotic transition. *Genome Biol*
828 **16**:94. doi:10.1186/s13059-015-0659-4
829
830 Lee C-Y, Wilkinson BD, Siegrist SE, Wharton RP, Doe CQ. 2006. Brat Is a Miranda
831 Cargo Protein that Promotes Neuronal Differentiation and Inhibits Neuroblast Self-
832 Renewal. *Dev Cell* **10**:441–449. doi:10.1016/j.devcel.2006.01.017
833
834 Littleton J, Bellen H. 1994. Genetic and phenotypic analysis of thirteen essential genes
835 in cytological interval 22F1-2; 23B1-2 reveals novel genes required for neural
836 development in Drosophila. *Genetics* **138**:111–23.
837
838 Loedige I, Jakob L, Treiber T, Ray D, Stotz M, Treiber N, Hennig J, Cook KB, Morris Q,
839 Hughes TR, Engelmann JC, Krahn MP, Meister G. 2015. The Crystal Structure of the
840 NHL Domain in Complex with RNA Reveals the Molecular Basis of Drosophila Brain-
841 Tumor-Mediated Gene Regulation. *Cell Reports* **13**:1206–1220.
842 doi:10.1016/j.celrep.2015.09.068
843
844 Loedige I, Stotz M, Qamar S, Kramer K, Hennig J, Schubert T, Löffler P, Längst G,
845 Merkl R, Urlaub H, Meister G. 2014. The NHL domain of BRAT is an RNA-binding
846 domain that directly contacts the hunchback mRNA for regulation. *Gene Dev* **28**:749–
847 764. doi:10.1101/gad.236513.113
848
849 Luschnig S, Moussian B, Krauss J, Desjeux I, Perkovic J, Nüsslein-Volhard C. 2004. An

F1 Genetic Screen for Maternal-Effect Mutations Affecting Embryonic Pattern Formation in Drosophila melanogaster. *Genetics* **167**:325–342. doi:10.1534/genetics.167.1.325

Luttrell SM, Gotting K, Ross E, Alvarado A, Swalla BJ. 2016. Head regeneration in hemichordates is not a strict recapitulation of development. *Dev Dynam* **245**:1159–1175. doi:10.1002/dvdy.24457

Mader MM, Cameron DA. 2004. Photoreceptor Differentiation during Retinal Development, Growth, and Regeneration in a Metamorphic Vertebrate. *J Neurosci* **24**:11463–11472. doi:10.1523/jneurosci.3343-04.2004

Martín R, Pinal N, Morata G. 2017. Distinct regenerative potential of trunk and appendages of Drosophila mediated by JNK signalling. *Development* **144**:dev.155507. doi:10.1242/dev.155507

McClure KD, Schubiger G. 2008. A screen for genes that function in leg disc regeneration in Drosophila melanogaster. *Mech Develop* **125**:67–80. doi:10.1016/j.mod.2007.10.003

McCusker CD, Gardiner DM. 2013. Positional Information Is Reprogrammed in Blastema Cells of the Regenerating Limb of the Axolotl (Ambystoma mexicanum). *Plos One* **8**:e77064. doi:10.1371/journal.pone.0077064

873 Micchelli C, Rulifson E, Blair S. 1997. The function and regulation of cut expression on
874 the wing margin of Drosophila: Notch, Wingless and a dominant negative role for Delta
875 and Serrate. *Dev Camb Engl* **124**:1485–95.

876 Mitchell NC, Johanson TM, Cranna NJ, Er ALJ, Richardson HE, Hannan RD, Quinn LM.
877 2010. Hfp inhibits Drosophila myc transcription and cell growth in a TFIIH/Hay-
878 dependent manner. *Development* **137**:2875–2884. doi:10.1242/dev.049585
879

880 Mukherjee S, Tucker-Burden C, Zhang C, Moberg K, Read R, Hadjipanayis C, Brat DJ.
881 2016. Drosophila Brat and Human Ortholog TRIM3 Maintain Stem Cell Equilibrium and
882 Suppress Brain Tumorigenesis by Attenuating Notch Nuclear Transport. *Cancer Res*
883 **76**:2443–2452. doi:10.1158/0008-5472.can-15-2299
884

885 Muneoka K, Bryant SV. 1982. Evidence that patterning mechanisms in developing and
886 regenerating limbs are the same. *Nature* **298**:298369a0. doi:10.1038/298369a0
887

888 Myohara M. 2004. Differential tissue development during embryogenesis and
889 regeneration in an annelid. *Dev Dynam* **231**:349–358. doi:10.1002/dvdy.20115
890

891 Nakamura T, Mito T, Bando T, Ohuchi H, Noji S. 2007. Molecular and Cellular Basis of
892 Regeneration and Tissue Repair. *Cell Mol Life Sci* **65**:64. doi:10.1007/s00018-007-
893 7432-0
894

895 Narbonne-Reveau K, Maurange C. 2019. Developmental regulation of regenerative

potential in Drosophila by ecdysone through a bistable loop of ZBTB transcription factors. *Plos Biol* **17**:e3000149. doi:10.1371/journal.pbio.3000149

Ng M, Diaz-Benjumea F, Cohen S. 1995. Nubbin encodes a POU-domain protein required for proximal-distal patterning in the Drosophila wing. *Dev Camb Engl* **121**:589–99.

Nicklas S, Otto A, Wu X, Miller P, Stelzer S, Wen Y, Kuang S, Wrogemann K, Patel K, Ding H, Schwamborn JC. 2012. TRIM32 Regulates Skeletal Muscle Stem Cell Differentiation and Is Necessary for Normal Adult Muscle Regeneration. *Plos One* **7**:e30445. doi:10.1371/journal.pone.0030445

Parks AL, Cook KR, Belvin M, Dompe NA, Fawcett R, Huppert K, Tan LR, Winter CG, Bogart KP, Deal JE, Deal-Herr ME, Grant D, Marcinko M, Miyazaki WY, Robertson S, Shaw KJ, Tabios M, Vysotskaia V, Zhao L, Andrade RS, Edgar KA, Howie E, Killpack K, Milash B, Norton A, Thao D, Whittaker K, Winner MA, Friedman L, Margolis J, Singer MA, Kopczynski C, Curtis D, Kaufman TC, Plowman GD, Duyk G, Francis-Lang HL. 2004. Systematic generation of high-resolution deletion coverage of the Drosophila melanogaster genome. *Nat Genet* **36**:ng1312. doi:10.1038/ng1312

Pierce SB, Yost C, Britton JS, Loo LW, Flynn EM, Edgar BA, Eisenman RN. 2004. dMyc is required for larval growth and endoreplication in Drosophila. *Development* **131**:2317–2327. doi:10.1242/dev.01108

Roensch K, Tazaki A, Chara O, Tanaka EM. 2013. Progressive Specification Rather than Intercalation of Segments During Limb Regeneration. *Science* **342**:1375–1379. doi:10.1126/science.1241796

Saj A, Arziman Z, Stempfle D, van Belle W, Sauder U, Horn T, Dürrenberger M, Paro R, Boutros M, Merdes G. 2010. A Combined Ex Vivo and In Vivo RNAi Screen for Notch Regulators in Drosophila Reveals an Extensive Notch Interaction Network. *Dev Cell* **18**:862–876. doi:10.1016/j.devcel.2010.03.013

Schubiger M, Sustar A, Schubiger G. 2010. Regeneration and transdetermination: The role of wingless and its regulation. *Dev Biol* **347**:315–324. doi:10.1016/j.ydbio.2010.08.034

Schuster KJ, Smith-Bolton RK. 2015. Taranis Protects Regenerating Tissue from Fate Changes Induced by the Wound Response in Drosophila. *Dev Cell* **34**:119–128. doi:10.1016/j.devcel.2015.04.017

Schwamborn JC, Berezikov E, Knoblich JA. 2009. The TRIM-NHL Protein TRIM32 Activates MicroRNAs and Prevents Self-Renewal in Mouse Neural Progenitors. *Cell* **136**:913–925. doi:10.1016/j.cell.2008.12.024

Skinner A, Khan S, Smith-Bolton RK. 2015. Trithorax regulates systemic signaling

942 during Drosophila imaginal disc regeneration. *Development* **142**:3500–3511.
943 doi:10.1242/dev.122564
944
945 Smith-Bolton RK, Worley MI, Kanda H, Hariharan IK. 2009. Regenerative Growth in
946 Drosophila Imaginal Discs Is Regulated by Wingless and Myc. *Dev Cell* **16**:797–809.
947 doi:10.1016/j.devcel.2009.04.015
948
949 Sonoda J, Wharton RP. 2001. Drosophila Brain Tumor is a translational repressor.
950 *Gene Dev* **15**:762–773. doi:10.1101/gad.870801
951
952 Stathakis D, Pentz E, Freeman M, Kullman J, Hankins G, Pearlson N, Wright T. 1995.
953 The genetic and molecular organization of the Dopa decarboxylase gene cluster of
954 Drosophila melanogaster. *Genetics* **141**:629–55.
955
956 Sun G, Irvine KD. 2014. Chapter Four Control of Growth During Regeneration. *Curr Top*
957 *Dev Biol* **108**:95–120. doi:10.1016/b978-0-12-391498-9.00003-6
958
959 Sun G, Irvine KD. 2011. Regulation of Hippo signaling by Jun kinase signaling during
960 compensatory cell proliferation and regeneration, and in neoplastic tumors. *Dev Biol*
961 **350**:139–151. doi:10.1016/j.ydbio.2010.11.036
962
963 Takahashi K, Yamanaka S. 2006. Induction of Pluripotent Stem Cells from Mouse
964 Embryonic and Adult Fibroblast Cultures by Defined Factors. *Cell* **126**:663–676.

965 doi:10.1016/j.cell.2006.07.024

966

967 Tasaki J, Shibata N, Sakurai T, Agata K, Umesono Y. 2011. Role of c-Jun N-terminal

968 kinase activation in blastema formation during planarian regeneration. *Dev Growth*

969 *Differ* **53**:389–400. doi:10.1111/j.1440-169x.2011.01254.x

970

971 Verghese S, Su T. 2017. STAT, Wingless, and Nurf-38 determine the accuracy of

972 regeneration after radiation damage in Drosophila. *Plos Genet* **13**:e1007055.

973 doi:10.1371/journal.pgen.1007055

974

975 Vizcaya-Molina E, Klein CC, Serras F, Mishra RK, Guigó R, Corominas M. 2018.

976 Damage-responsive elements in Drosophila regeneration. *Genome Res* **28**:1852–1866.

977 doi:10.1101/gr.233098.117

978

979 Vonesch S, Lamparter D, Mackay TF, Bergmann S, Hafen E. 2016. Genome-Wide

980 Analysis Reveals Novel Regulators of Growth in Drosophila melanogaster. *Plos Genet*

981 **12**:e1005616. doi:10.1371/journal.pgen.1005616

982

983 Watanabe-Fukunaga R, Iida S, Shimizu Y, Nagata S, Fukunaga R. 2005. SEI family of

984 nuclear factors regulates p53-dependent transcriptional activation. *Genes Cells* **10**:851–

985 860. doi:10.1111/j.1365-2443.2005.00881.x

986

987 Wehner D, Cizelsky W, Vasudevaro M, Özhan G, Haase C, Kagermeier-Schenk B,

988 Röder A, Dorsky RI, Moro E, Argenton F, Kühl M, Weidinger G. 2014. Wnt/β-Catenin
989 Signaling Defines Organizing Centers that Orchestrate Growth and Differentiation of the
990 Regenerating Zebrafish Caudal Fin. *Cell Reports* **6**:467–481.
991 doi:10.1016/j.celrep.2013.12.036
992
993 Wright T, Bewley G, Sherald A. 1976. The genetics of dopa decarboxylase in
994 Drosophila melanogaster. II. Isolation and characterization of dopa-decarboxylase-
995 deficient mutants and their relationship to the alpha-methyl-dopa-hypersensitive
996 mutants. *Genetics* **84**:287–310.
997
998 Wright TR, Beermann W, Marsh LJ, Bishop CP, Steward R, Black BC, Tomsett AD,
999 Wright EY. 1981. The genetics of dopa decarboxylase in Drosophila melanogaster.
1000 *Chromosoma* **83**:45–58. doi:10.1007/bf00286015
1001
1002 Wu CD, Johnston LA. 2010. Control of Wing Size and Proportions by Drosophila Myc.
1003 *Genetics* **184**:199–211. doi:10.1534/genetics.109.110379

Figure 1

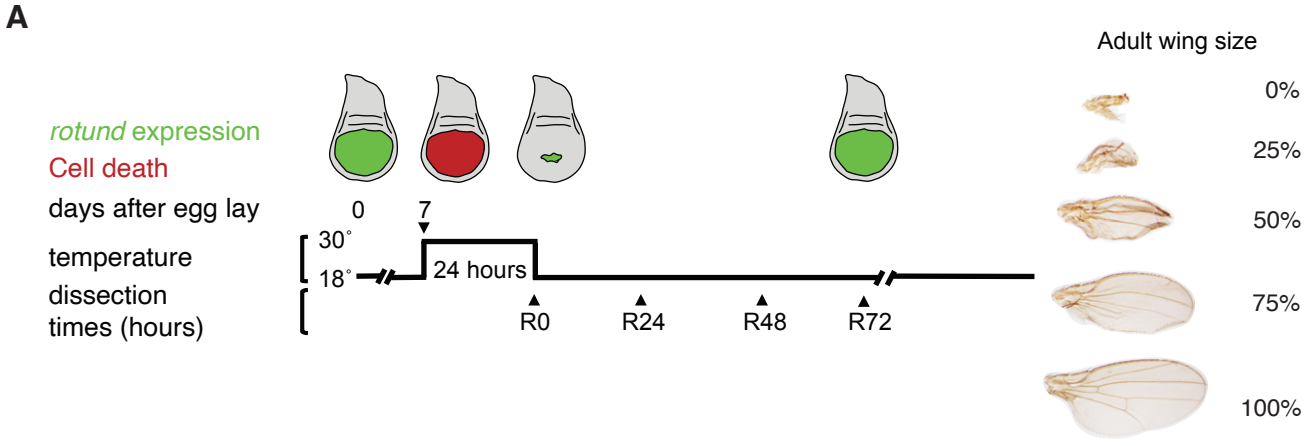
A
Adult wing size
0%
25%
50%
75%
100%
rotund expression
Cell death
days after egg lay
0
7
temperature
30˚
18˚
24 hours
dissection times (hours)
R0
R24
R48
R72

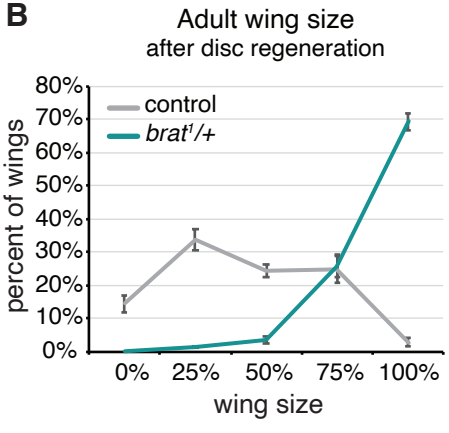
B
Adult wing size
after disc regeneration
percent of wings
control
brat1/+
80%
70%
60%
50%
40%
30%
20%
10%
0%
0%
25%
50%
75%
100%
wing size

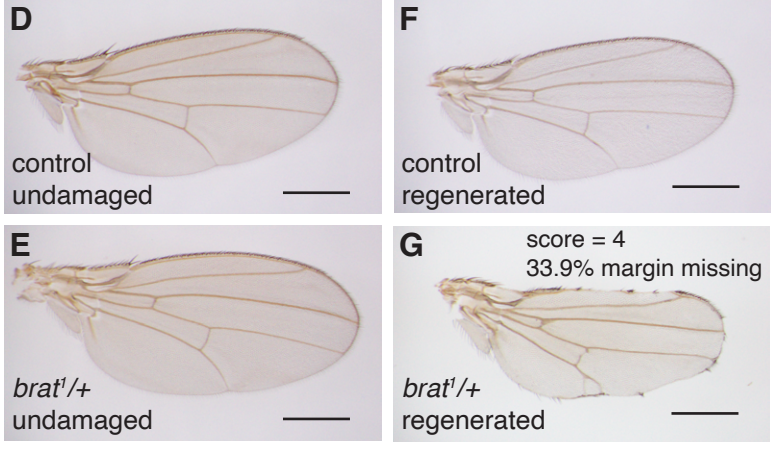
D
control
undamaged
F
control
regenerated
E
brat1/+
undamaged
G
score = 4
33.9% margin missing
brat1/+
regenerated

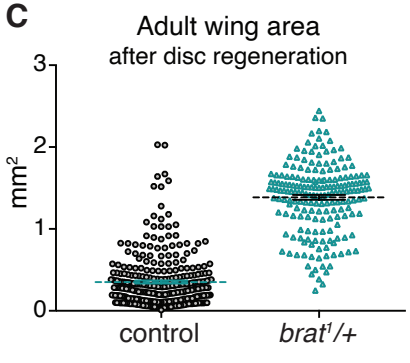
C
Adult wing area
after disc regeneration
mm2
3
2
1
0
control
brat1/+

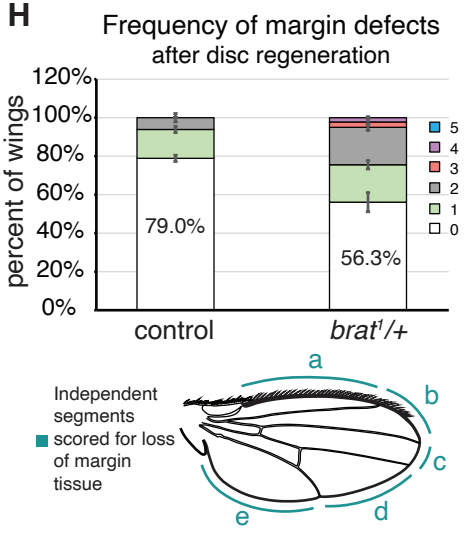
H
Frequency of margin defects
after disc regeneration
percent of wings
120%
100%
80%
60%
40%
20%
0%
79.0%
56.3%
5
4
3
2
1
0
control
brat1/+
Independent segments scored for loss of margin tissue
a
b
c
d
e

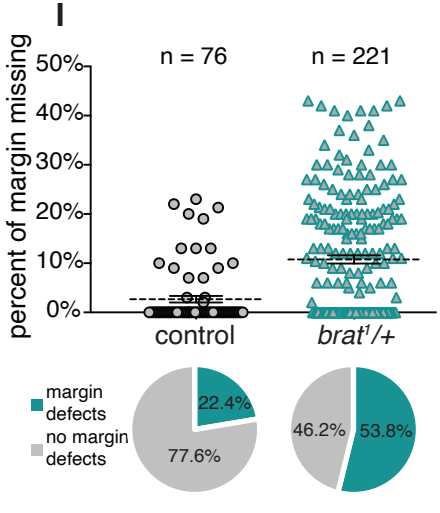
I
percent of margin missing
50%
40%
30%
20%
10%
0%
n = 76
n = 221
control
brat1/+
margin defects
no margin defects
22.4%
77.6%
46.2%
53.8%

Figure 1. Enhanced regenerative growth and wing margin cell-fate specification defects in *brat*^{1}/+ during regeneration.

(A) The protocol used to study regeneration. Animals were raised at 18°C and shifted to 30°C for 24 hours during early third-instar larval development on day 7 after egg lay (AEL). Larvae were returned to 18°C and were dissected at the time points noted during recovery (R) or allowed to pupariate and eclose. Representative wings depicting the range of adult wing sizes observed after regeneration compared to the size of a normal wing are shown. (B) Adult wing sizes observed after disc regeneration for control (w^{1118}) (n = 317) and *brat*^{1}/+ (n = 208) wings, from three independent experiments. (C) Adult wing area after disc regeneration, measured using ImageJ after mounting and imaging wings, for control (w^{1118}) (n = 309) and *brat*^{1}/+ (n = 195) wings. p = 2.5158E-119. Wings in (C) are from the same experiments as (B). Note that number of wings in (C) is less for both control and *brat*^{1}/+ due to some wings being damaged during the mounting process. (D) Undamaged control (w^{1118}) wing. (E) Undamaged *brat*^{1}/+ wing. (F) Adult control (w^{1118}) wing after disc regeneration. (G) Adult *brat*^{1}/+ wing after disc regeneration. (H) Frequency of margin defects seen in adult wings after disc regeneration for control (w^{1118}) (n = 93) and *brat*^{1}/+ (n = 218) wings, from three independent experiments. The wing margin was divided into five segments based on where the veins intersect the margin as shown in the diagram. Each wing was scored for the number of segments that had some margin tissue missing, with wings with a perfectly intact margin scoring at zero. Wing shown in (G) had tissue missing in four segments. (I) Margin tissue lost as a percentage of total wing perimeter for control (w^{1118}) (n = 76) and *brat*^{1}/+ (n = 221) wings. p = 9.947E-08. The margin perimeter and

the length of margin tissue lost were measured using ImageJ after mounting and imaging wings. Wings in (I) are from the same experiments as (H). Note that number of wings in the two quantifications is different because we did not quantify wings with length <1.1 mm for males and <1.7 mm for females, to ensure analysis was being carried out on nearly fully regenerated wings. (I). Percentage of wings with no defects fell from 79.0% to 77.6% for control and from 56.3% to 53.8% for *brat*^{1}/+ wings due to the increased ability to detect lost margin tissue at the higher magnification and resolution achieved by imaging the wings. Wing shown in (G) had 33.9% of margin tissue missing. Error bars mark standard error of the mean (SEM). Student's T-test used for statistical analyses. Scale bars are 0.5 mm.

Figure 2

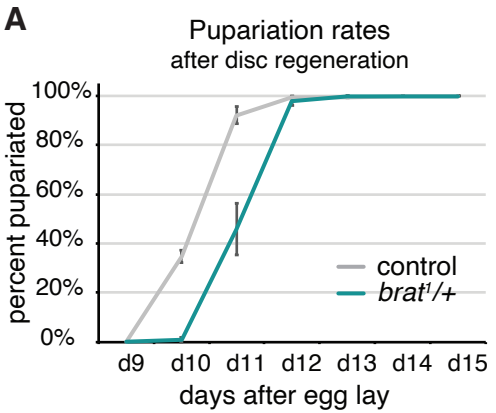
A
Pupariation rates
after disc regeneration
100%
80%
60%
40%
20%
0%
percent pupariated
d9
d10
d11
d12
d13
d14
d15
days after egg lay
control
brat1/+

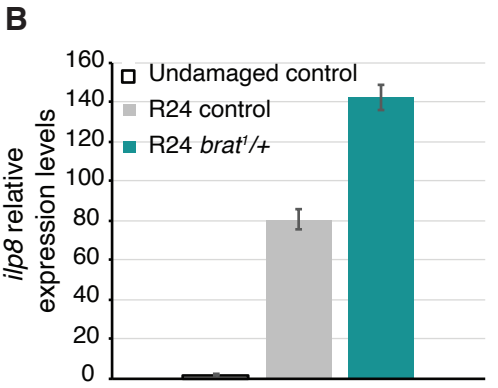
B
160
140
120
100
80
60
40
20
0
ilp8 relative
expression levels
Undamaged control
R24 control
R24 brat1/+

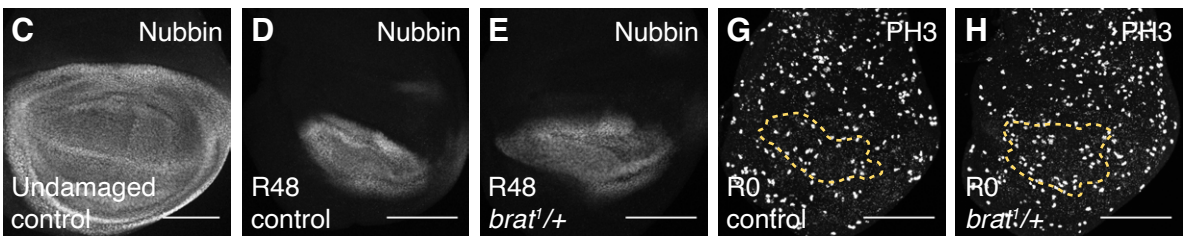
C
Nubbin
Undamaged
control
D
Nubbin
R48
control
E
Nubbin
R48
brat1/+
G
PH3
R0
control
H
PH3
R0
brat1/+

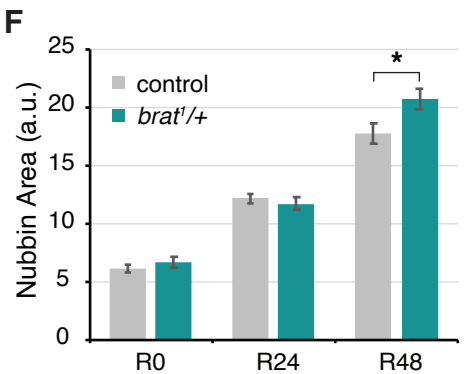
F
25
20
15
10
5
0
Nubbin Area (a.u.)
control
brat1/+
*
R0
R24
R48

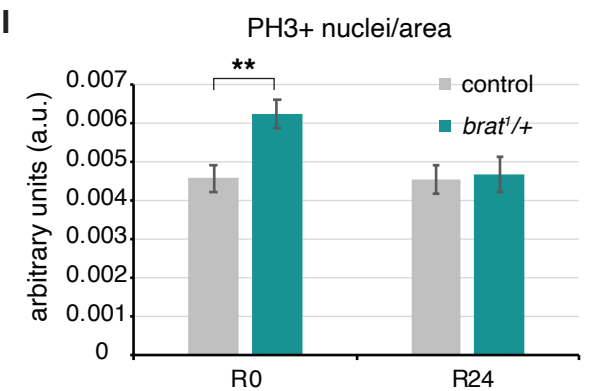
I
PH3+ nuclei/area
0.007
0.006
0.005
0.004
0.003
0.002
0.001
0
arbitrary units (a.u.)
**
control
brat1/+
R0
R24

Figure 2. *brat*^{1}/+ animals have a regenerative growth advantage.

(A) Pupariation rates after disc regeneration for control (w^{1118}) (n = 384) and *brat*^{1}/+ (n = 107) animals, from three independent experiments. (B) Relative expression levels of *ilp8* for undamaged control, R24 control (w^{1118}) and R24 *brat*^{1}/+ discs. (C) Anti-Nubbin immunostaining in an undamaged control disc. (D-E) Anti-Nubbin immunostaining in an R48 control (w^{1118}) disc (D), and an R48 *brat*^{1}/+ disc (E). (F) Quantification of area of Nubbin-expressing cells for control (w^{1118}) and *brat*^{1}/+ discs at R0 (n = 10 and 10), R24 (n = 12 and 12) and R48 (n = 10 and 10). * $p < 0.03$. (G-H) Anti-PH3 immunostaining in an R0 control (w^{1118}) disc (G), and an R0 *brat*^{1}/+ disc (H). The yellow dashed lines outline the Nubbin-expressing wing pouch. (I) PH3-positive nuclei were counted within the regenerating tissue as marked by Anti-Nubbin co-immunostaining. Quantification of PH3-positive nuclei in Nubbin area for control (w^{1118}) and *brat*^{1}/+ discs at R0 (n = 16 and 18) and R24 (n = 15 and 16). ** $p < 0.002$. Error bars represent SEM. Student's T-test used for statistical analyses. Scale bars are 100 μm.

Figure 3

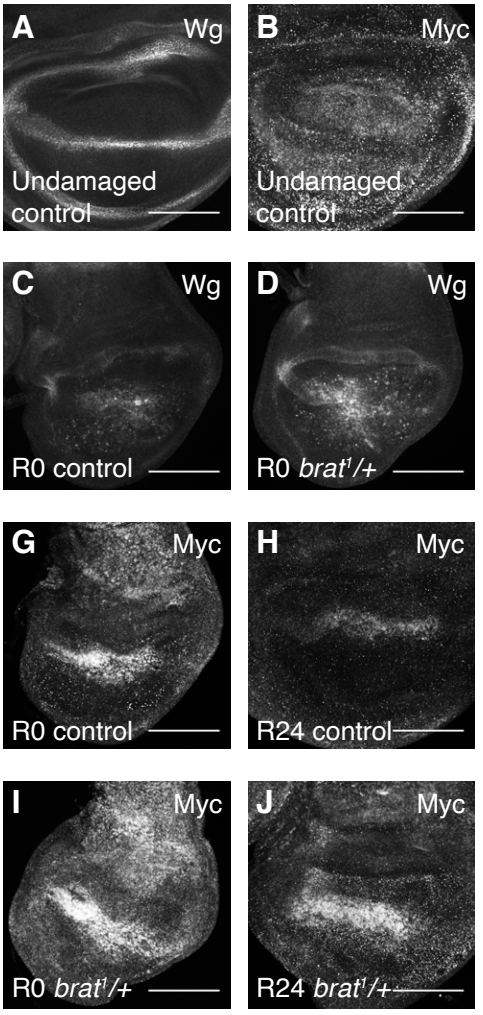
A
Wg
Undamaged control
B
Myc
Undamaged control
C
Wg
R0 control
D
Wg
R0 brat¹/+
G
Myc
R0 control
H
Myc
R24 control
I
Myc
R0 brat¹/+
J
Myc
R24 brat¹/+

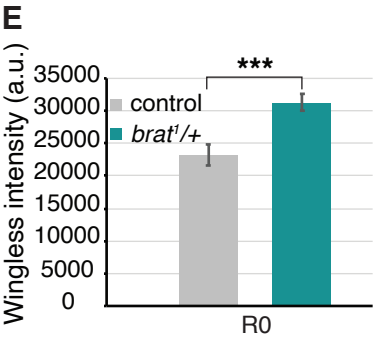
E
Wingless intensity (a.u.)
35000
30000
25000
20000
15000
10000
5000
0
control
brat¹/+
***
R0

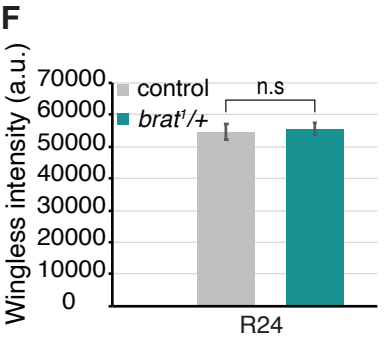
F
Wingless intensity (a.u.)
70000
60000
50000
40000
30000
20000
10000
0
control
brat¹/+
n.s
R24

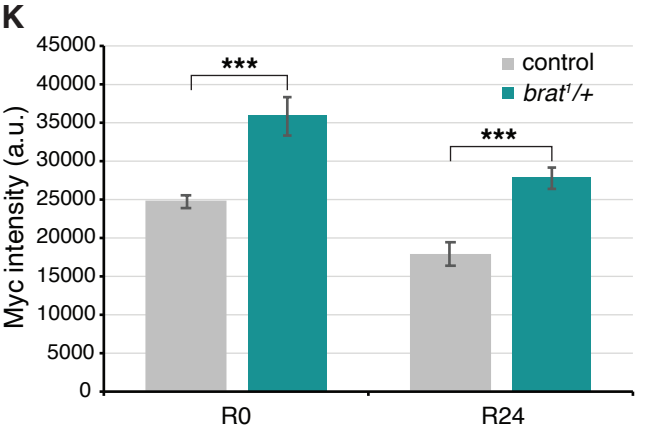
K
Myc intensity (a.u.)
45000
40000
35000
30000
25000
20000
15000
10000
5000
0
control
brat¹/+
***
***
R0
R24

Figure 3. *brat*^{1}/+ animals experience elevated regeneration signaling.

(A) Anti-Wg immunostaining in an undamaged control (*w*^{1118}) disc. (B) Anti-Myc immunostaining in an undamaged control (*w*^{1118}) disc. (C-D) Anti-Wg immunostaining in an R0 control (*w*^{1118}) disc (C) and an R0 *brat*^{1}/+ disc (D). (E) Quantification of Wg fluorescence intensity in R0 control (*w*^{1118}) (n = 13) and R0 *brat*^{1}/+ (n = 17) discs. *** $p < 0.0006$. (F) Quantification of Wg fluorescence intensity in R24 control (*w*^{1118}) (n = 12) and R24 *brat*^{1}/+ (n = 11) discs. Area for fluorescence intensity measurement was defined by the Wg expression domain in the wing pouch. (G-J) Anti-Myc immunostaining in an R0 control (*w*^{1118}) disc (G), an R24 control (*w*^{1118}) disc (H), an R0 *brat*^{1}/+ disc (I) and an R24 *brat*^{1}/+ disc (J). (K) Quantification of Myc fluorescence intensity in R0 control (*w*^{1118}) (n = 13), R0 *brat*^{1}/+ (n = 12), R24 control (*w*^{1118}) (n = 13), and R24 *brat*^{1}/+ (n = 12) discs. Area for fluorescence intensity measurement was defined by the elevated Myc expression domain in the wing pouch. R0 *** $p < 0.0003$, R24 *** $p < 0.0001$. Error bars represent SEM. Student's T-test used for statistical analyses. Scale bars are 100 μm.

Figure 4

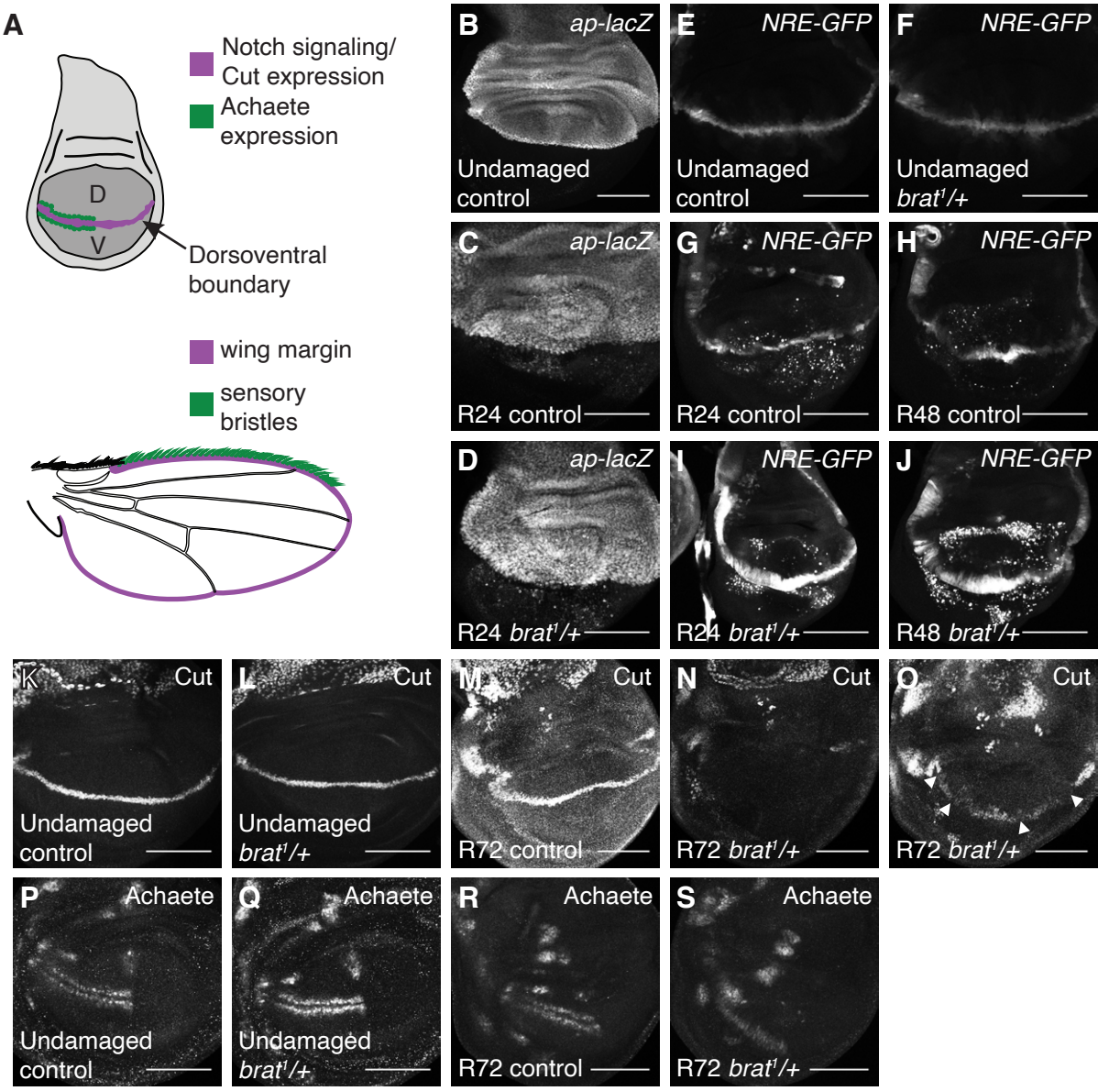
A
Notch signaling/
Cut expression
Achaete
expression
D
V
Dorsoventral
boundary
wing margin
sensory
bristles
B ap-lacZ
Undamaged
control
E NRE-GFP
Undamaged
control
F NRE-GFP
Undamaged
brat1/+
C ap-lacZ
R24 control
G NRE-GFP
R24 control
H NRE-GFP
R48 control
D ap-lacZ
R24 brat1/+
I NRE-GFP
R24 brat1/+
J NRE-GFP
R48 brat1/+
K Cut
Undamaged
control
L Cut
Undamaged
brat1/+
M Cut
R72 control
N Cut
R72 brat1/+
O Cut
R72 brat1/+
P Achaete
Undamaged
control
Q Achaete
Undamaged
brat1/+
R Achaete
R72 control
S Achaete
R72 brat1/+

Figure 4. *Brat* regulates margin cell-fate specification.

(A) Drawings of a wing imaginal disc and an adult wing. D = dorsal and V = ventral compartments of the wing disc, with the dorsoventral boundary marked in purple. Notch signaling and Cut expression are present at the dorsoventral boundary, which forms the adult wing margin, also marked in purple. Achaete-expressing cells, marked in green, give rise to the sensory bristles at the anterior half of the margin in the adult wing, also marked in green. (B) *ap-lacZ* expression in an undamaged control disc from a third-instar *ap-lacZ/CyO* animal. (C-D) *ap-lacZ* expression in an R24 control (w^{1118}) disc (C) and an R24 $brat^{1}$/+ disc (D). (E-F) *NRE-GFP* expression in an undamaged control (w^{1118}) disc (E) and an undamaged $brat^{1}$/+ disc (F). (G-J) *NRE-GFP* expression in an R0 control (w^{1118}) disc (G), an R24 control (w^{1118}) disc (H), an R0 $brat^{1}$/+ disc (I) and an R24 $brat^{1}$/+ disc (J). (K-L) Anti-Ct immunostaining in an undamaged control (w^{1118}) disc (K) and an undamaged $brat^{1}$/+ disc (L). (M-O) Anti-Ct immunostaining in an R72 control (w^{1118}) disc (M) and an R72 $brat^{1}$/+ discs (N-O). Arrowheads point to loss of Ct expression in (O). (P-Q) Anti-Ac immunostaining in an undamaged control (w^{1118}) disc (P) and an undamaged $brat^{1}$/+ disc (Q). (R-S) Anti-Ac immunostaining in an R72 control (w^{1118}) disc (R) and an R72 $brat^{1}$/+ disc (S). Scale bars are 100 μm.

Figure 5

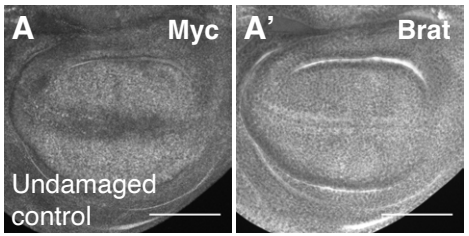
A
Myc
Undamaged
control

A'
Brat

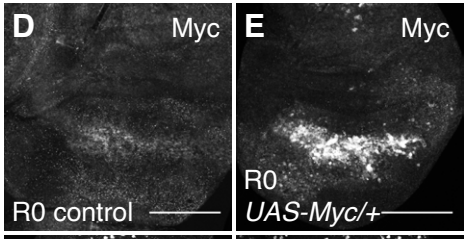
D
Myc
R0 control
E
Myc
R0
UAS-Myc/+

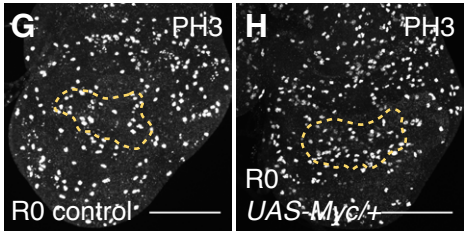
G
PH3
R0 control
H
PH3
R0
UAS-Myc/+

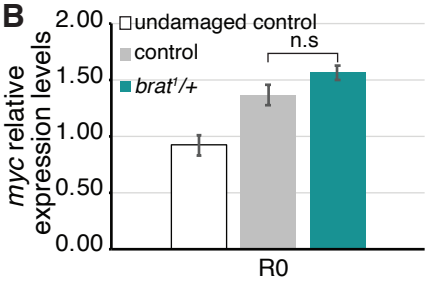
B
myc relative expression levels
2.00
1.50
1.00
0.50
0.00
undamaged control
control
brat¹/+
n.s
R0

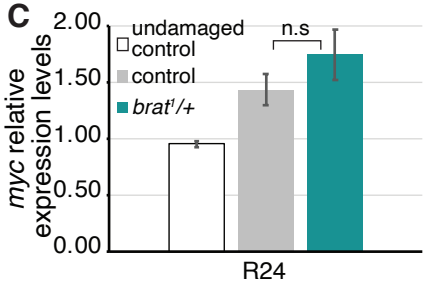
C
myc relative expression levels
2.00
1.50
1.00
0.50
0.00
undamaged control
control
brat¹/+
n.s
R24

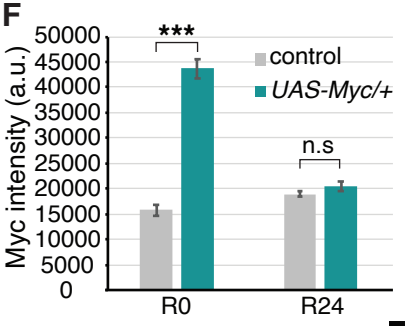
F
Myc intensity (a.u.)
50000
45000
40000
35000
30000
25000
20000
15000
10000
5000
0
***
control
UAS-Myc/+
n.s
R0
R24

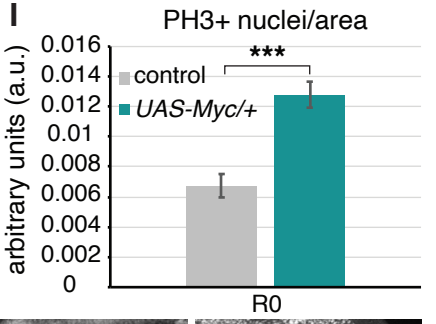
I
PH3+ nuclei/area
arbitrary units (a.u.)
0.016
0.014
0.012
0.01
0.008
0.006
0.004
0.002
0
***
control
UAS-Myc/+
R0

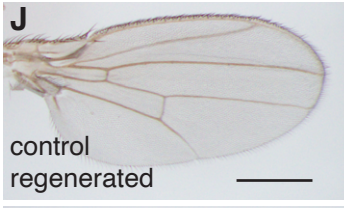
J
control
regenerated

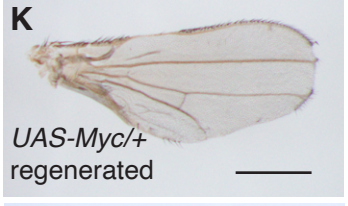
K
UAS-Myc/+
regenerated

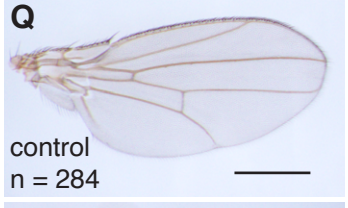
Q
control
n = 284

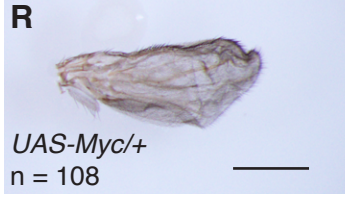
R
UAS-Myc/+
n = 108

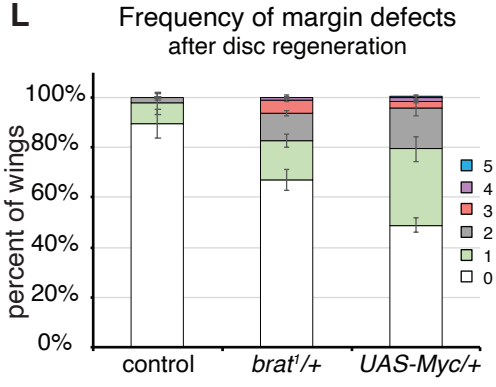
L
Frequency of margin defects
after disc regeneration
percent of wings
100%
80%
60%
40%
20%
0%
5
4
3
2
1
0
control
brat¹/+
UAS-Myc/+

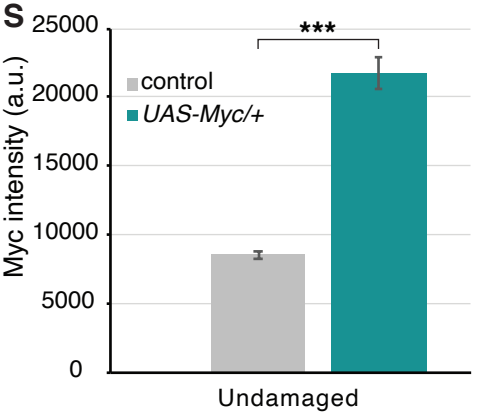
S
Myc intensity (a.u.)
25000
20000
15000
10000
5000
0
***
control
UAS-Myc/+
Undamaged

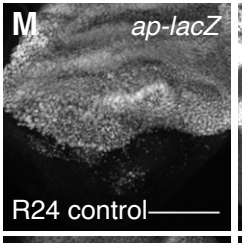
M
ap-lacZ
R24 control

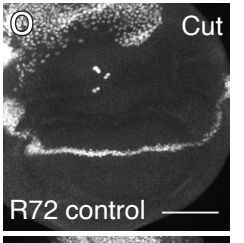
O
Cut
R72 control

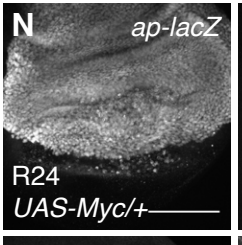
N
ap-lacZ
R24
UAS-Myc/+

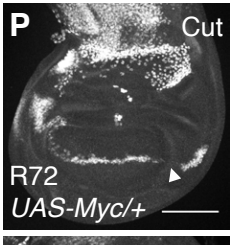
P
Cut
R72
UAS-Myc/+

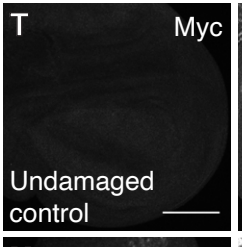
T
Myc
Undamaged
control

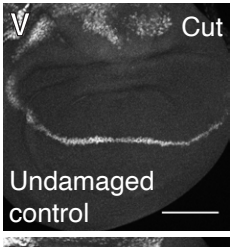
V
Cut
Undamaged
control

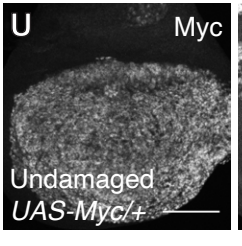
U
Myc
Undamaged
UAS-Myc/+

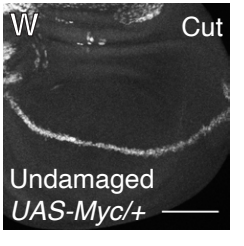
W
Cut
Undamaged
UAS-Myc/+

Figure 5. High Myc expression causes margin defects.

(A-A') Anti-Myc and Anti-Brat co-immunostaining in an undamaged control disc. *rnGAL4, GAL80^{ts}/attP2* animals were shifted to 30°C on day 7 AEL and dissected 24 hours later. (B-C) Relative expression levels of *myc* for undamaged control, regenerating control (*w^{1118}*), and regenerating *brat^{1}*/+ discs at R0 (B) and R24 (C). P values for comparison between regenerating control and *brat^{1}*/+ discs: p > 0.1 at R0, and p > 0.3 at R24. (D-E) Anti-Myc immunostaining in an R0 control (*w^{1118}*) disc (D) and an R0 *UAS-Myc/+* disc (E). (F) Quantification of Myc fluorescence intensity in R0 control (*w^{1118}*) (n = 13), R0 *UAS-Myc/+* (n = 12), R24 control (*w^{1118}*) (n = 13), and R24 *UAS-Myc/+* (n = 12) discs. Area for fluorescence intensity measurement was defined by the elevated Myc expression domain in the wing pouch. *** p = 1.2E-11. (G-H) Anti-PH3 immunostaining in an R0 control (*w^{1118}*) disc (G), and an R0 *UAS-Myc/+* disc (H). The yellow dashed lines outline the Nubbin-expressing wing pouch. (I) PH3-positive nuclei were counted within the regenerating wing pouch as marked by Anti-Nubbin co-immunostaining. Quantification of PH3-positive nuclei in the Nubbin area for R0 control (*w^{1118}*) (n = 15) and *UAS-Myc/+* (n = 15) discs. *** p < 0.00002. (J) Adult control (*w^{1118}*) wing after disc regeneration. (K) Adult *UAS-Myc/+* wing after disc regeneration. (L) Frequency of margin defects, as quantified in Figure 1H, seen in adult wings after disc regeneration for control (*w^{1118}*) (n = 134), *brat^{1}*/+ (n = 193) and *UAS-Myc/+* (n = 200) wings, from three independent experiments. (M-N) *ap-lacZ* expression in an R24 control (*w^{1118}*) disc (M) and an R24 *UAS-Myc/+* disc (N). (O-P) Anti-Ct immunostaining in an R72 control (*w^{1118}*) disc (O) and an R72 *UAS-Myc/+* disc (P). (Q) Adult undamaged control (*+; rnGAL4,GAL80ts/+*) wing from animals shifted to 30°C on day 7 AEL and

maintained at 30°C until eclosion. (R) Adult wing from discs continuously overexpressing Myc from day 7 AEL onwards (*UAS-Myc/+; rnGAL4, GAL80ts/+)*. (S) Quantification of Myc fluorescence intensity in undamaged discs dissected 31 hours after animals were shifted to 30°C on day 7 AEL. Control (+*; rnGAL4,GAL80ts/*+) (n = 14) and *UAS-Myc (UAS-Myc/+; rnGAL4, GAL80ts/+)* (n = 14). Area for fluorescence intensity measurement was defined by the Myc expression domain in the wing pouch. *** p = 1.2E-11. (T-U) Anti-Myc immunostaining in an undamaged control disc (T) and an undamaged *UAS-Myc/*+ disc (U). (V-W) Anti-Ct immunostaining in an undamaged control disc (V) and an undamaged *UAS-Myc/*+ disc (W). Error bars represent SEM. Student's T-test used for statistical analyses. Scale bars are 100 μm. Scale bars for adult wings are 0.5 mm.

Figure 6

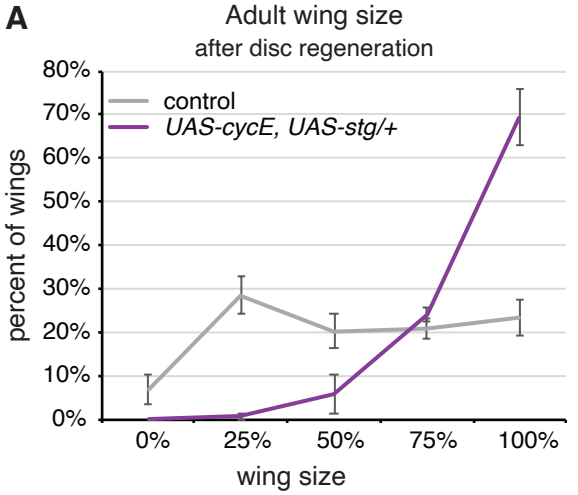
A
Adult wing size
after disc regeneration
control
UAS-cycE, UAS-stg/+
percent of wings
80%
70%
60%
50%
40%
30%
20%
10%
0%
0%
25%
50%
75%
100%
wing size

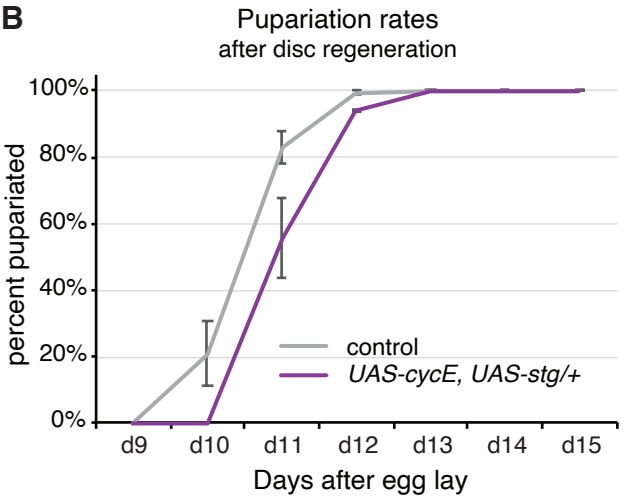
B
Pupariation rates
after disc regeneration
percent pupariated
100%
80%
60%
40%
20%
0%
control
UAS-cycE, UAS-stg/+
d9
d10
d11
d12
d13
d14
d15
Days after egg lay

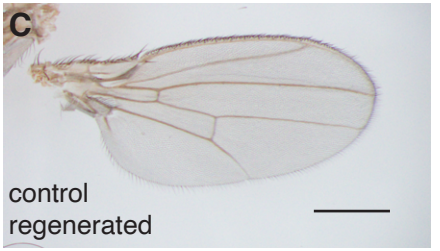
C
control
regenerated

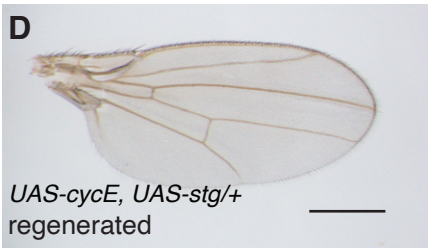
D
UAS-cycE, UAS-stg/+
regenerated

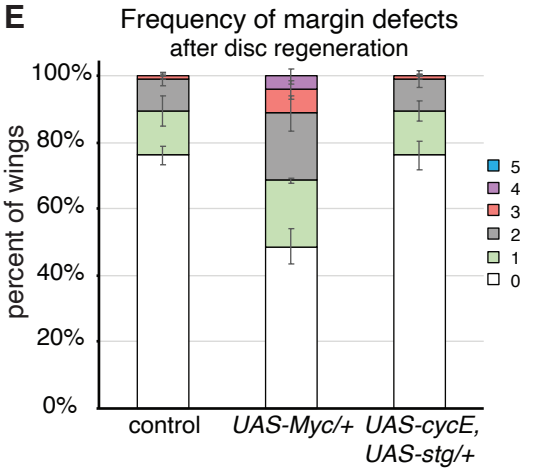
E
Frequency of margin defects
after disc regeneration
percent of wings
100%
80%
60%
40%
20%
0%
5
4
3
2
1
0
control
UAS-Myc/+
UAS-cycE,
UAS-stg/+

Figure 6. Overexpression of cell cycle genes does not cause patterning defects.

(A) Adult wing sizes observed after disc regeneration for control (w^{1118}) (n = 280) and *UAS-cycE, UAS-stg/+* (n = 194) wings, from three independent experiments. (B) Pupariation rates after disc regeneration for control (w^{1118}) (n = 174) and *UAS-cycE, UAS-stg/+* (n = 115) wings, from three independent experiments. (C) Adult control (w^{1118}) wing after disc regeneration. (D) Adult *UAS-cycE, UAS-stg/+* wing after disc regeneration. (E) Frequency of margin defects seen in adult wings after disc regeneration for control (w^{1118}) (n = 118), *UAS-Myc/+* (n = 146), and *UAS-cycE, UAS-stg/+* (n = 188) wings, from three independent experiments. Error bars represent SEM. Scale bars for adult wings are 0.5 mm.

Figure 7

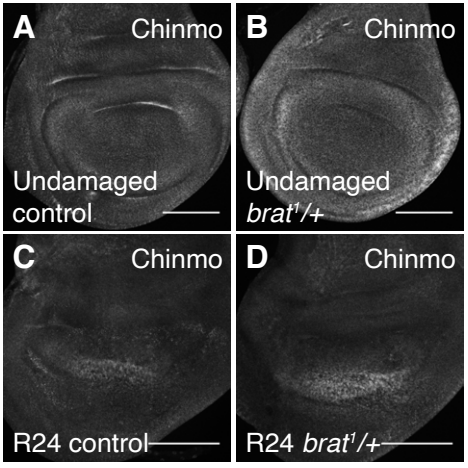
A
Chinmo
Undamaged
control
B
Chinmo
Undamaged
brat1/+
C
Chinmo
R24 control
D
Chinmo
R24 brat1/+

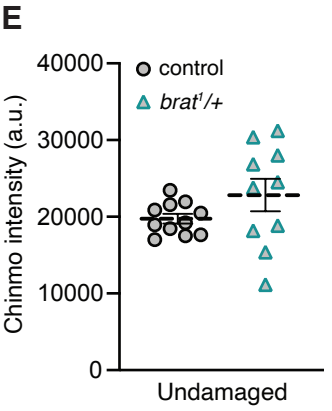
E
40000
30000
20000
10000
0
Chinmo intensity (a.u.)
control
brat1/+
Undamaged

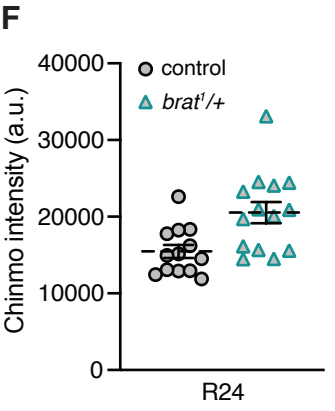
F
40000
30000
20000
10000
0
Chinmo intensity (a.u.)
control
brat1/+
R24

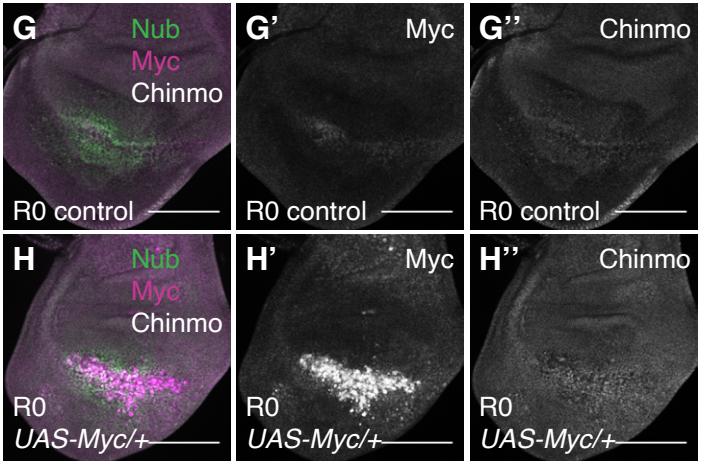
G
Nub
Myc
Chinmo
R0 control
G'
Myc
R0 control
G''
Chinmo
R0 control
H
Nub
Myc
Chinmo
R0
UAS-Myc/+
H'
Myc
R0
UAS-Myc/+
H''
Chinmo
R0
UAS-Myc/+

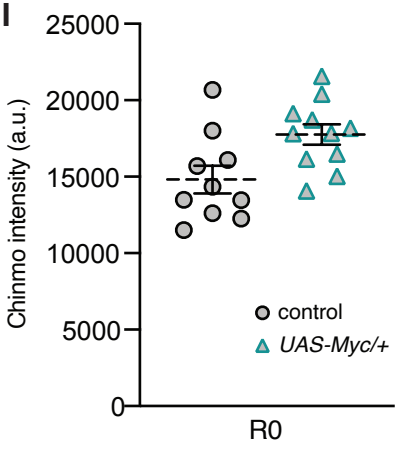
I
25000
20000
15000
10000
5000
0
Chinmo intensity (a.u.)
control
UAS-Myc/+
R0

Figure 7. Chinmo levels are elevated in *brat*^{1}/+ and Myc-overexpressing regenerating discs.

(A-B) Anti-Chinmo immunostaining in an undamaged control (*w*^{1118}) disc (A) and an undamaged *brat*^{1}/+ disc (B). (C-D) Anti-Chinmo immunostaining in an R24 control (*w*^{1118}) disc (C) and an R24 *brat*^{1}/+ disc (D). (E) Quantification of Chinmo fluorescence intensity in undamaged control (*w*^{1118}) (n = 11) and undamaged *brat*^{1}/+ (n = 10) discs. (F) Quantification of Chinmo fluorescence intensity in R24 control (*w*^{1118}) (n = 13) and R24 *brat*^{1}/+ (n = 14) discs. $p < 0.006$. Area for fluorescence intensity measurement was defined by the elevated Chinmo expression domain in the wing pouch. (G) Merge of anti-Nubbin, anti-Myc and anti-Chinmo immunostaining in an R0 control (*w*^{1118}) disc. (G'-G'') Same disc as (G) showing anti-Myc and anti-Chinmo immunostaining, respectively. (H) Merge of anti-Nubbin, anti-Myc and anti-Chinmo immunostaining in an R0 *brat*^{1}/+ disc. (H'-H'') Same disc as (H) showing anti-Myc and anti-Chinmo immunostaining, respectively. (I) Quantification of Chinmo fluorescence intensity in R0 control (*w*^{1118}) (n = 10) and R0 *UAS-Myc*/+ (n = 11) discs. $p < 0.02$. Area for fluorescence intensity measurement was defined by the elevated Myc expression domain in the wing pouch. Error bars represent SEM. Student's T-test used for statistical analyses. Scale bars are 100 μm.

Figure 8

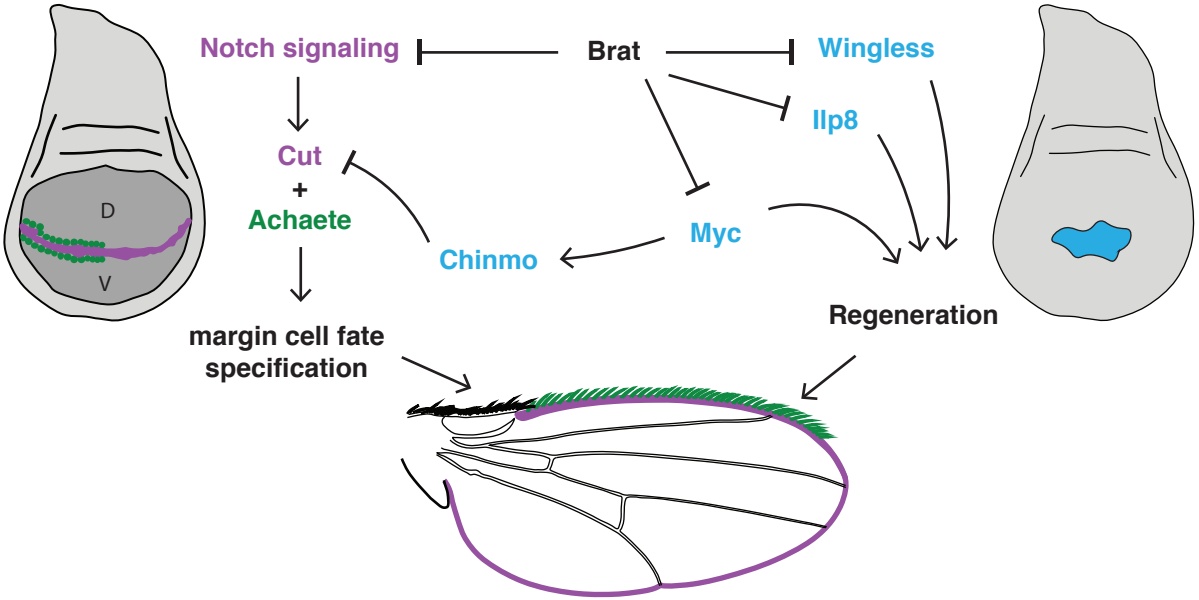
Notch signaling
Brat
Wingless
Ilp8
Cut
+
Achaete
Chinmo
Myc
D
V
margin cell fate
specification
Regeneration

Figure 8. Brat restricts pro-regeneration factors and ensures correct margin cell-fate specification.

Model describing the network of Brat targets in the regenerating wing imaginal disc. Importantly, Brat restricts Myc levels, limiting expression of Myc's targets, including Chinmo, to allow correct margin cell-fate specification.

Figure S1

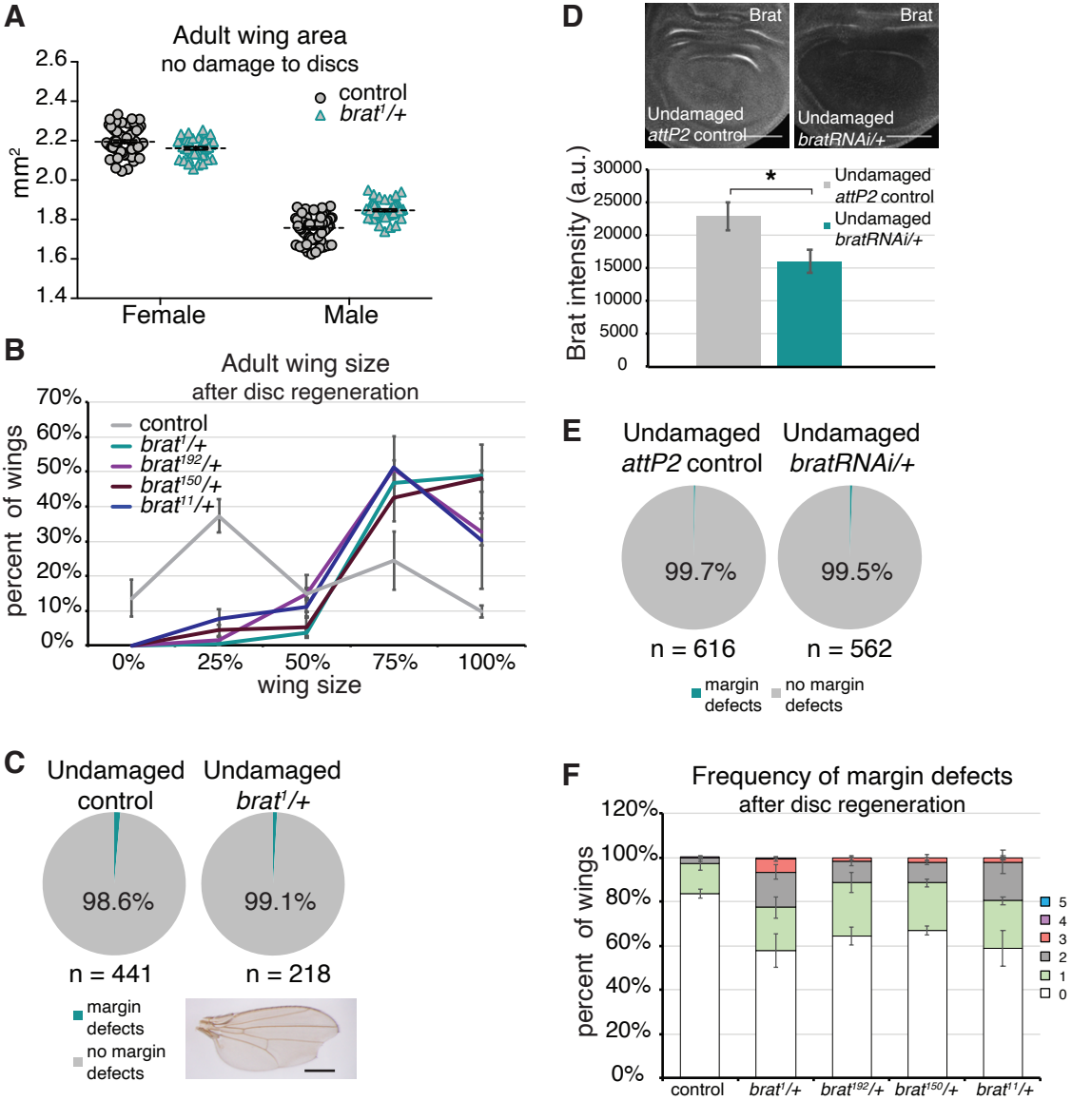
A
Adult wing area
no damage to discs
control
brat1/+
mm2
2.6
2.4
2.2
2.0
1.8
1.6
1.4
Female
Male
B
Adult wing size
after disc regeneration
control
brat1/+
brat192/+
brat150/+
brat11/+
percent of wings
70%
60%
50%
40%
30%
20%
10%
0%
0%
25%
50%
75%
100%
wing size
C
Undamaged
control
Undamaged
brat1/+
98.6%
99.1%
n = 441
n = 218
margin defects
no margin defects
D
Brat
Brat
Undamaged
attP2 control
Undamaged
bratRNAi/+
Brat intensity (a.u.)
30000
25000
20000
15000
10000
5000
0
*
Undamaged
attP2 control
Undamaged
bratRNAi/+
E
Undamaged
attP2 control
Undamaged
bratRNAi/+
99.7%
99.5%
n = 616
n = 562
margin defects
no margin defects
F
Frequency of margin defects
after disc regeneration
percent of wings
120%
100%
80%
60%
40%
20%
0%
control
brat1/+
brat192/+
brat150/+
brat11/+
5
4
3
2
1
0

Figure S1. Loss of *brat* does not cause enhanced growth or margin defects during normal development (Related to Figure 1).

(A) Adult wing area measured using ImageJ after mounting and imaging wings, for undamaged control (w^{1118}) (n = 63 female and 70 male) and $brat^{1}$/+ (n = 38 female and 48 male) wings. *rnGAL4, GAL80^{ts}/TM6B* females were crossed to w^{1118} or $brat^{1}$/*SM6-TM6B* males and taken through the protocol shown in Figure 1A. (B) Adult wing sizes after disc regeneration for control (w^{1118}) (n = 599), $brat^{1}$/+ (n = 199), $brat^{192}$/+ (n = 237), $brat^{150}$/+ (n = 235) and $brat^{11}$/+ (n = 188) wings, from three independent experiments. (C) Margin defects detected in adult wings from undamaged control (w^{1118}) and $brat^{1}$/+ discs. *rnGAL4, GAL80^{ts}/TM6B* females were crossed to w^{1118} or $brat^{1}$/*SM6-TM6B* males and taken through the protocol shown in Figure 1A. Margin defects detected in the undamaged wings were never as severe as the ones seen in $brat^{1}$/+ wings after disc regeneration. A representative wing with margin defects is shown. (D) Anti-Brat immunostaining in undamaged control (*attP2*) and *bratRNAi*/+ discs. *rnGAL4, GAL80^{ts}/TM6B* females were crossed to *attP2* or *bratRNAi* males. Larvae were kept at 18°C and shifted to 30°C on day 7 AEL. Discs were dissected 24 hours after the shift to 30°C. Quantification of Brat fluorescence intensity in undamaged control *(attP2*) (n = 15) and *bratRNAi*/+ (n = 15) discs. Area for fluorescence intensity measurement was defined by wing pouch morphology and Anti-Myc co-immunostaining. * p = 0.02. (E) Margin defects detected in adult wings from undamaged control (*attP2*) and *bratRNAi* dics. *rnGAL4, GAL80^{ts}/TM6B* females were crossed to *attP2* or *bratRNAi* males. Larvae were kept at 18°C and shifted to 30°C on day 7 AEL and kept there until eclosion. (F) Frequency of margin defects seen in adult wings after disc regeneration for control

(w^{1118}) (n = 240), $brat^{1}$/+ (n = 191), $brat^{192}$/+ (n = 196), $brat^{150}$/+ (n = 213) and $brat^{11}$/+ (n = 152) wings. Wings in (G) are from the same experiments as (B). Error bars represent SEM. Student's T-test used for statistical analyses. Scale bars are 100 μm. Scale bars for adult wings are 0.5 mm.

Figure S2

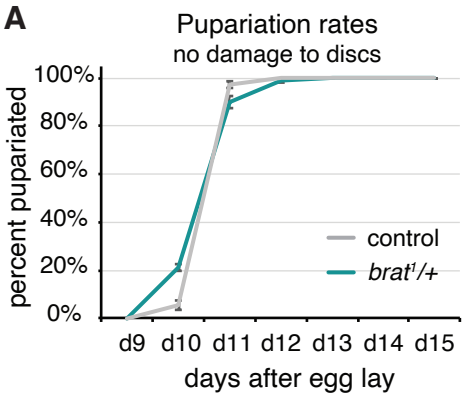
A
Pupariation rates
no damage to discs
100%
80%
60%
40%
20%
0%
percent pupariated
d9 d10 d11 d12 d13 d14 d15
days after egg lay
control
brat1/+

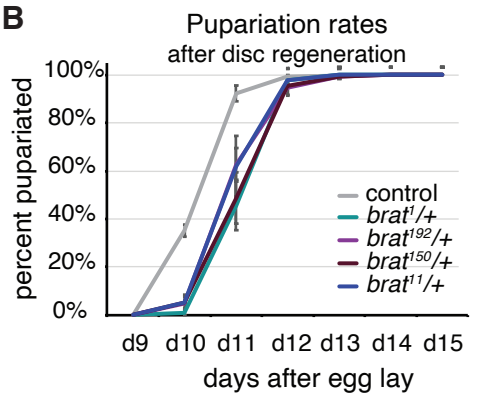
B
Pupariation rates
after disc regeneration
100%
80%
60%
40%
20%
0%
percent pupariated
d9 d10 d11 d12 d13 d14 d15
days after egg lay
control
brat1/+
brat192/+
brat150/+
brat11/+

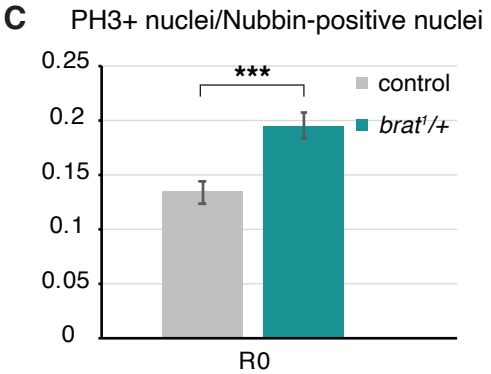
C
PH3+ nuclei/Nubbin-positive nuclei
0.25
0.2
0.15
0.1
0.05
0
***
control
brat1/+
R0

Figure S2. Loss of *brat* delays pupariation in a regeneration-specific manner (Related to Figure 2).

(A) Pupariation rates in undamaged control (w^{1118}) (n = 221) and $brat^{1}$/+ (n = 110) animals, from three independent experiments. (B) Pupariation rates after disc regeneration for control (w^{1118}) (n = 384), $brat^{1}$/+ (n = 107), $brat^{192}$/+ (n = 131), $brat^{150}$/+ (n = 114) and $brat^{11}$/+ (n = 113) animals. Pupariation rates are from the same experiments as in Figure 2A. (C) PH3-positive nuclei were counted within the regenerating tissue as marked by Anti-Nubbin co-immunostaining. Total number of nuclei were also counted in the Nubbin expressing region. Ratio of PH3-positive nuclei and total Nubbin-positive nuclei for control (w^{1118}) and $brat^{1}$/+ discs at R0 (n = 16 and 18). *** $p < 0.0005$. Error bars represent SEM. Student's T-test used for statistical analyses. Error bars represent SEM.

Figure S3

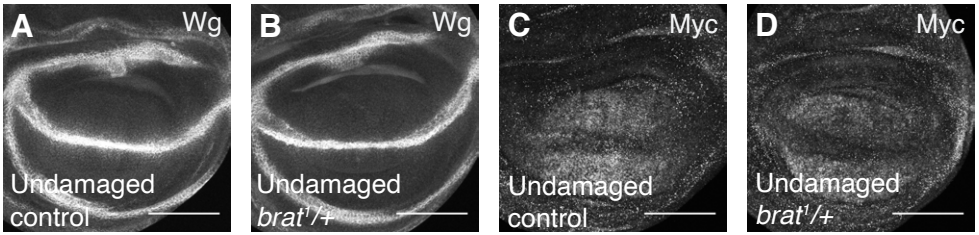
A
Wg
Undamaged
control
B
Wg
Undamaged
brat1/+
C
Myc
Undamaged
control
D
Myc
Undamaged
brat1/+

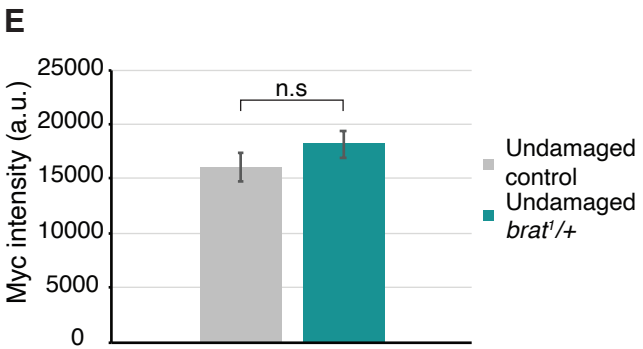
E
25000
20000
15000
10000
5000
0
Myc intensity (a.u.)
n.s
Undamaged
control
Undamaged
brat1/+

Figure S3. Effects of loss of *brat* on Wg and Myc expression are regeneration-specific (Related to Figure 3).

(A-B) Anti-Wg immunostaining in an undamaged control (w^{1118}) disc (A) and an undamaged $brat^{1}$/+ disc (B). (C-D) Anti-Myc immunostaining in an undamaged control (w^{1118}) disc (C) and an undamaged $brat^{1}$/+ disc (D). (E) Quantification of Myc fluorescence intensity in undamaged control (w^{1118}) (n = 10) and $brat^{1}$/+ (n = 10) discs. Area for fluorescence intensity measurement was defined by wing pouch morphology and the elevated Myc expression domain in the wing pouch. Error bars represent SEM. Student's T-test used for statistical analyses. Scale bars are 100 μm.

Figure S4

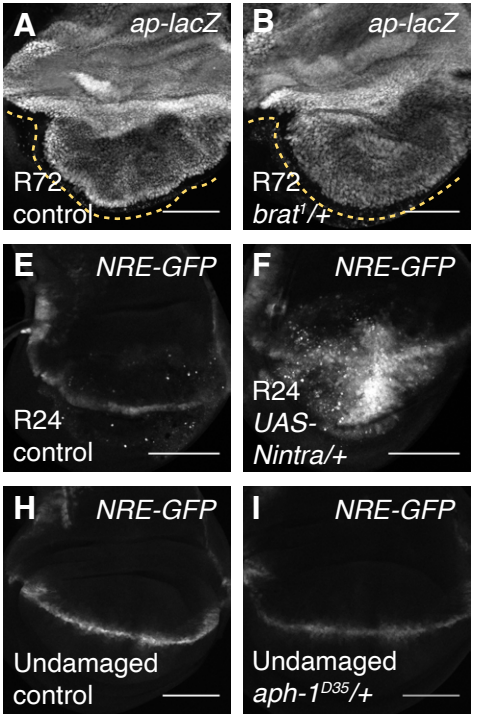
A
ap-lacZ
R72
control
B
ap-lacZ
R72
brat¹/+
E
NRE-GFP
R24
control
F
NRE-GFP
R24
UAS-
Nintra/+
H
NRE-GFP
Undamaged
control
I
NRE-GFP
Undamaged
aph-1D35/+

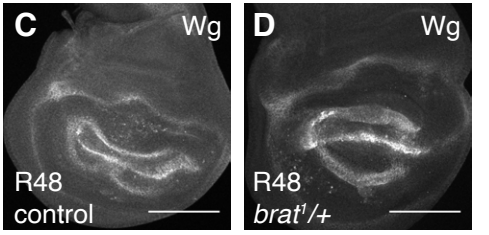
C
Wg
R48
control
D
Wg
R48
brat¹/+

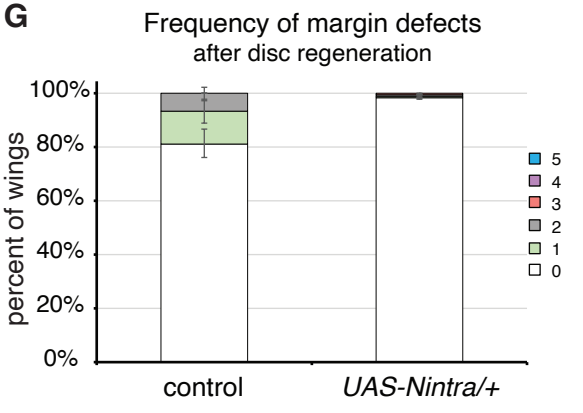
G
Frequency of margin defects
after disc regeneration
100%
80%
60%
40%
20%
0%
percent of wings
control
UAS-Nintra/+
5
4
3
2
1
0

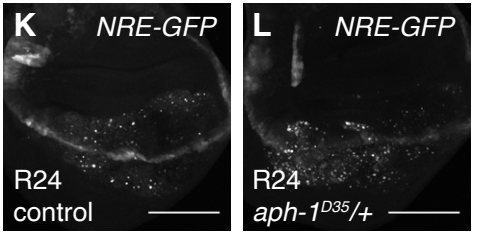
K
NRE-GFP
R24
control
L
NRE-GFP
R24
aph-1D35/+

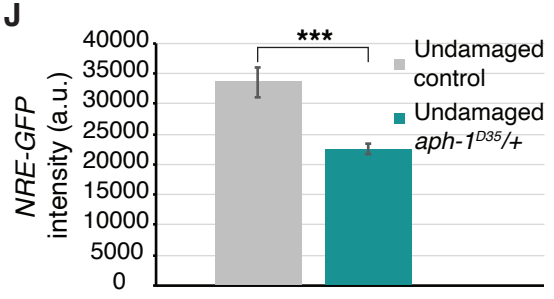
J
40000
35000
30000
25000
20000
15000
10000
5000
0
NRE-GFP
intensity (a.u.)
***
Undamaged
control
Undamaged
aph-1D35/+

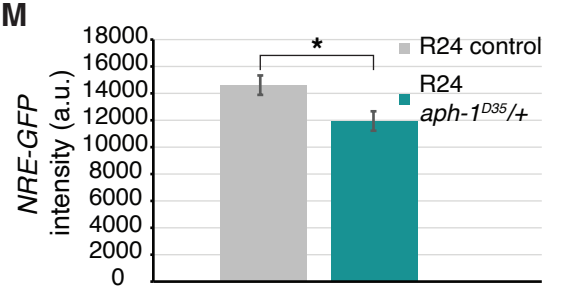
M
18000
16000
14000
12000
10000
8000
6000
4000
2000
0
NRE-GFP
intensity (a.u.)
*
R24 control
R24
aph-1D35/+

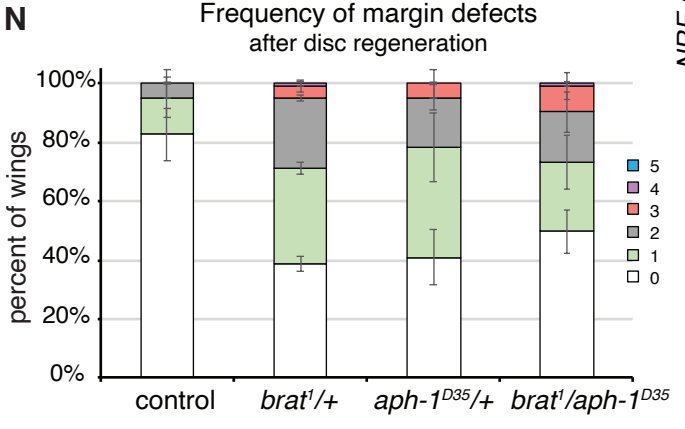
N
Frequency of margin defects
after disc regeneration
100%
80%
60%
40%
20%
0%
percent of wings
control
brat¹/+
aph-1D35/+
brat¹/aph-1D35
5
4
3
2
1
0

Figure S4. Elevated Notch signaling does not cause margin defects (Related to Figure 4).

(A-B) *ap-lacZ* expression in an R72 control (w^{1118}) disc (A) and an R72 $brat^{1}$/+ disc (B). Dashed yellow lines are drawn next to the DV boundary to highlight it. (C-D) Anti-Wg immunostaining in an R48 control (w^{1118}) disc (C) and an R48 $brat^{1}$/+ disc (D). (E-F) *NRE-GFP* expression in an R24 control (w^{1118}) disc (E) and an R24 *UAS-Nintra/+* disc (F). (G) Frequency of margin defects seen in adult wings after disc regeneration for control (w^{1118}) (n = 84) and *UAS-Nintra/+* (n = 357) wings, from five independent experiments. (H-I) *NRE-GFP* expression in an undamaged control (w^{1118}) disc (H) and an undamaged $aph\text{-}1^{D35}$/+ disc (I). *NRE-GFP*/+ and *NRE-GFP*/$aph\text{-}1^{D35}$ animals were raised at room temperature and dissected during third instar. (J) Quantification of GFP intensity in undamaged control (w^{1118}) (n = 15) and $aph\text{-}1^{D35}$/+ (n = 15) discs. *** $p < 0.0006$. (K-L) *NRE-GFP* expression in an R24 control (w^{1118}) disc (K) and an R24 $aph\text{-}1^{D35}$/+ disc (L). (M) Quantification of GFP intensity in R24 control (w^{1118}) (n = 13) and R24 $aph\text{-}1^{D35}$/+ (n = 11) discs. * $p < 0.02$. (N) Frequency of margin defects in adult wings after disc regeneration for control (w^{1118}) (n = 21), $brat^{1}$/+ (n = 137), $aph\text{-}1^{D35}$/+ (n = 38) and $brat^{1}/aph\text{-}1^{D35}$(n = 80) wings. Error bars represent SEM. Student's T-test used for statistical analyses. Scale bars are 100 μm.

Figure S5

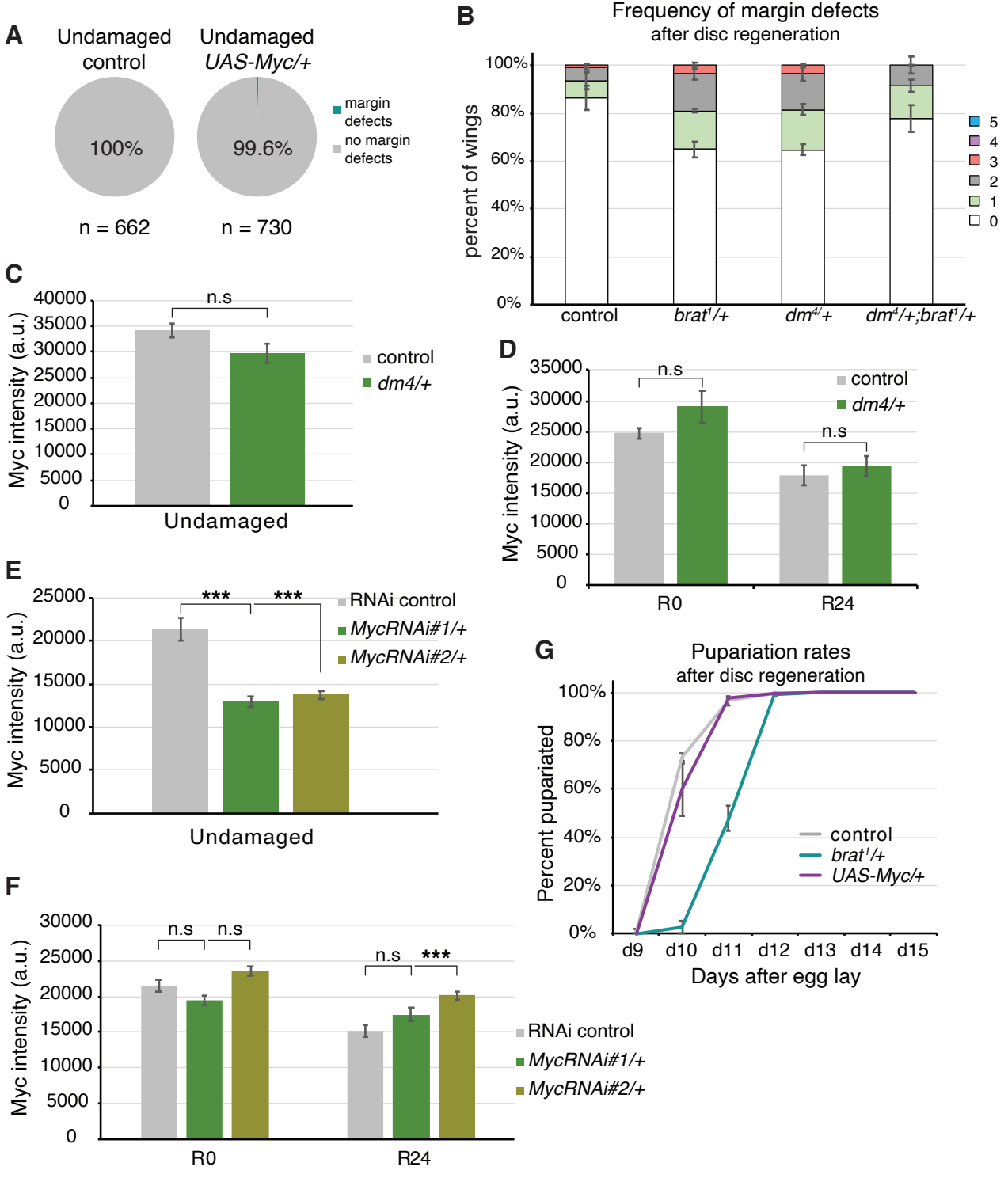
A
Undamaged control
Undamaged UAS-Myc/+
100%
99.6%
margin defects
no margin defects
n = 662
n = 730
B
Frequency of margin defects after disc regeneration
percent of wings
100%
80%
60%
40%
20%
0%
control
brat1/+
dm4/+
dm4/+;brat1/+
5
4
3
2
1
0
C
Myc intensity (a.u.)
40000
35000
30000
25000
20000
15000
10000
5000
0
n.s
control
dm4/+
Undamaged
D
Myc intensity (a.u.)
35000
30000
25000
20000
15000
10000
5000
0
n.s
n.s
control
dm4/+
R0
R24
E
Myc intensity (a.u.)
25000
20000
15000
10000
5000
0
***
***
RNAi control
MycRNAi#1/+
MycRNAi#2/+
Undamaged
F
Myc intensity (a.u.)
30000
25000
20000
15000
10000
5000
0
n.s
n.s
n.s
***
RNAi control
MycRNAi#1/+
MycRNAi#2/+
R0
R24
G
Pupariation rates after disc regeneration
Percent pupariated
100%
80%
60%
40%
20%
0%
control
brat1/+
UAS-Myc/+
d9
d10
d11
d12
d13
d14
d15
Days after egg lay

Figure S5. Compensatory regulation prevents reduction of Myc expression during regeneration (Related to Figure 5).

(A) Margin defects detected in adult wings from undamaged control (w^{1118}) and *UAS-Myc/+* discs. *rnGAL4, GAL80^{ts}/TM6B* females were crossed to w^{1118} or *UAS-Myc* males and taken through the protocol shown in Figure 1A. (B) Frequency of margin defects in adult wings after disc regeneration for control (w^{1118}) (n = 103), $brat^{1}$/+ (n = 203), dm^{4}/+ (n = 94) and dm^{4}/+; $brat^{1}$/+ (n = 94) wings, from three independent experiments. (C) Quantification of Myc fluorescence intensity in undamaged control (w^{1118}) (n = 12) and dm^{4}/+ (n = 11) discs. w^{1118} females were crossed to w^{1118} or *dm^{4}/FM7i, ActGFP* males and dissected when the animals were third instar. Area for fluorescence intensity measurement was defined by wing pouch morphology and the elevated Myc expression domain in the wing pouch. (D) Quantification of Myc fluorescence intensity in R0 control (w^{1118}) (n = 13), R0 dm^{4}/+ (n = 10), R24 control (w^{1118}) (n = 13), and R24 dm^{4}/+ (n = 10) discs. Area for fluorescence intensity measurement was defined by the elevated Myc expression domain in the wing pouch. (E) Quantification of Myc fluorescence intensity in undamaged control (VDRC genetic background line, called control) (n = 14), *MycRNAi#1/+* (n = 12), and *MycRNAi#2/+* (n = 13) discs. *rnGAL4, GAL80^{ts}/TM6B* females were crossed to the control, *MycRNAi#1*, or *MycRNAi#2* males. The animals were shifted to 30°C during early third instar and kept there for 28 hours then dissected. *MycRNAi#1/+* *** $p < 0.000007$, *MycRNAi#2/+* *** $p < 0.00002$. Area for fluorescence intensity measurement was defined by wing pouch morphology. (F) Quantification of Myc fluorescence intensity in R0 control (n = 13), R0 *MycRNAi#1/+* (n = 15), R0 *MycRNAi#2/+* (n = 13), R24 control (n = 13), R24 *MycRNAi#1/+* (n = 13), and R24

MycRNAi#2/+ (n = 13) discs. Fluorescence intensity was measured in the area marked by Anti-Nubbin immunostaining. *** $p < 0.00007$. (G) Pupariation rates after disc regeneration for control (w^{1118}) (n = 216), $brat^{1}$/+ (n = 114) and *UAS-Myc/+* (n = 209) animals, from three independent experiments. Error bars represent SEM. Student's T-test used for statistical analyses.

Figure S6

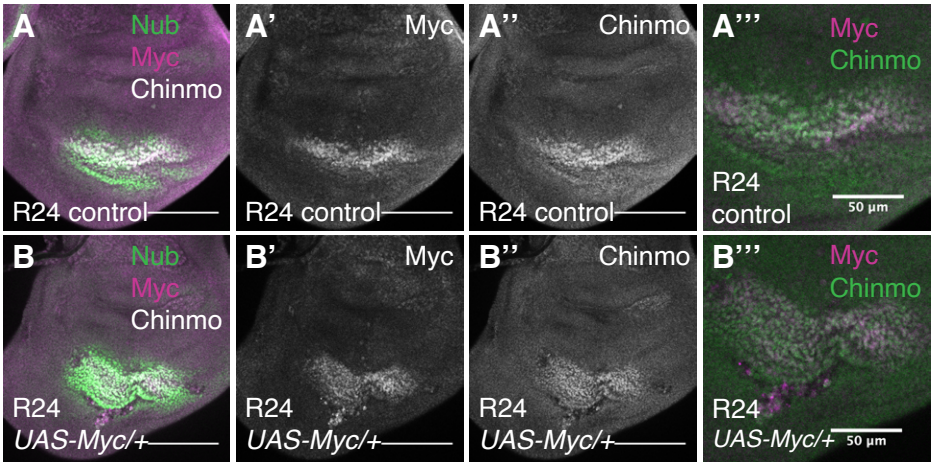
A
Nub
Myc
Chinmo
R24 control
A'
Myc
R24 control
A''
Chinmo
R24 control
A'''
Myc
Chinmo
R24
control
50 µm
B
Nub
Myc
Chinmo
R24
UAS-Myc/+
B'
Myc
R24
UAS-Myc/+
B''
Chinmo
R24
UAS-Myc/+
B'''
Myc
Chinmo
R24
UAS-Myc/+
50 µm

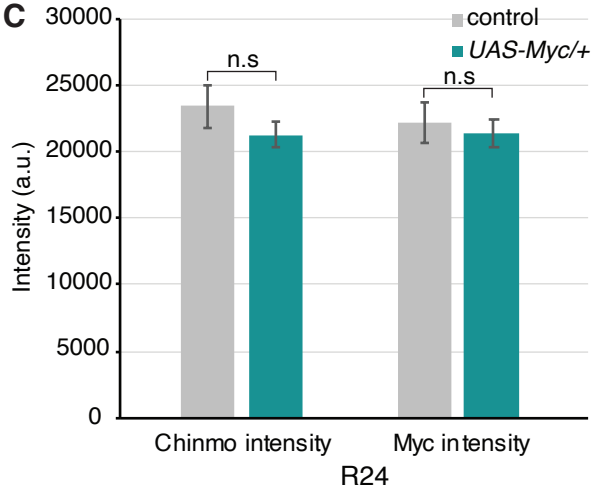
C
control
UAS-Myc/+
n.s
n.s
Intensity (a.u.)
30000
25000
20000
15000
10000
5000
0
Chinmo intensity
Myc intensity
R24

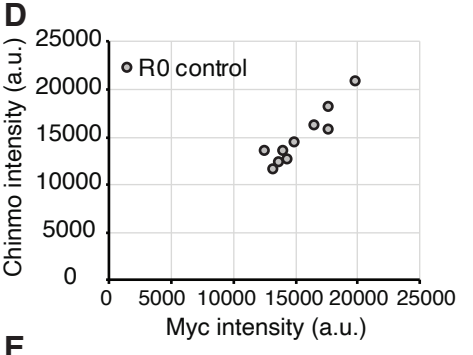
D
R0 control
Chinmo intensity (a.u.)
25000
20000
15000
10000
5000
0
0
5000
10000
15000
20000
25000
Myc intensity (a.u.)

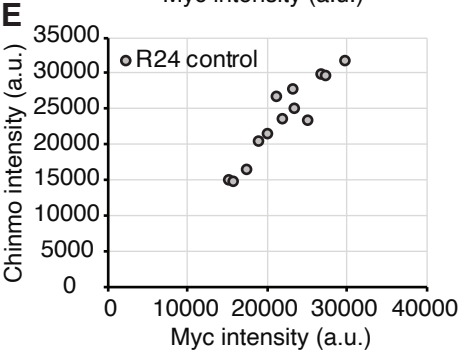
E
R24 control
Chinmo intensity (a.u.)
35000
30000
25000
20000
15000
10000
5000
0
0
10000
20000
30000
40000
Myc intensity (a.u.)

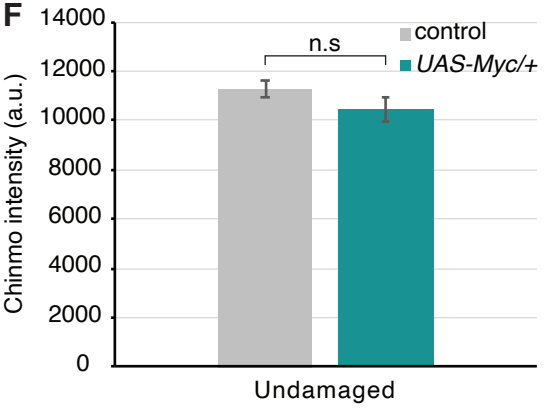
F
control
UAS-Myc/+
n.s
Chinmo intensity (a.u.)
14000
12000
10000
8000
6000
4000
2000
0
Undamaged

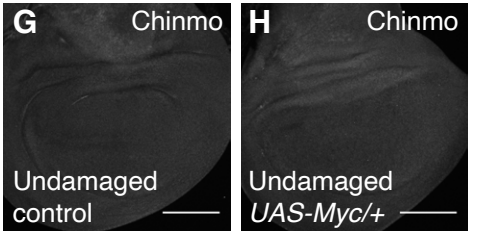
G
Chinmo
Undamaged
control
H
Chinmo
Undamaged
UAS-Myc/+

Figure S6. Myc regulates Chinmo expression (Related to Figure 7).

(A) Merge of anti-Nubbin, anti-Myc and anti-Chinmo immunostaining in an R24 control (w^{1118}) disc. (A'-A'') Same disc as (A) showing anti-Myc and anti-Chinmo immunostaining, respectively. (A''') Same disc as (A) showing an enlarged merge of anti-Myc and anti-Chinmo immunostaining. (B) Merge of anti-Nubbin, anti-Myc and anti-Chinmo immunostaining in an R24 *UAS-Myc/+* disc. (B'-B'') Same disc as (B) showing anti-Myc and anti-Chinmo immunostaining, respectively. (B''') Same disc as (B) showing an enlarged merge of anti-Myc and anti-Chinmo immunostaining. (C) Quantification of Chinmo and Myc fluorescence intensity in R24 control (w^{1118}) (n = 13) and R24 *UAS-Myc/+* (n = 14) discs. Area for fluorescence intensity measurement was defined by the elevated Myc expression domain in the wing pouch. Note that Myc and Chinmo expression co-localize. (D-E) Scatter plot showing correlation between Myc and Chinmo expression levels at R0 (D) and R24 (E). Pearson correlation coefficient for R0 = 0.93 and R24 = 0.94. (F) Quantification of Chinmo fluorescence intensity in undamaged discs dissected 31 hours after animals were shifted to 30°C on day 7 AEL. Control (*+;rnGAL4,GAL80ts/+*) (n = 14) and *UAS-Myc (UAS-Myc/+; rnGAL4, GAL80ts/+)* (n = 14). Area for fluorescence intensity measurement was defined by the Myc expression domain in the wing pouch. (G-H) Anti-Chinmo immunostaining in an undamaged control disc (G) and an undamaged *UAS-Myc/+* disc (H). Error bars represent SEM. Student's T-test used for statistical analyses. Scale bars are 100 μm, unless stated otherwise.